

# ZeroDVFS: Zero-Shot LLM-Guided Core and Frequency Allocation for Embedded Platforms

Mohammad Pivezhandi<sup>1</sup>, Mahdi Banisharif<sup>2</sup>, Abusayeed Saifullah<sup>3</sup>, and Ali Jannesari<sup>2</sup>

<sup>1</sup>Wayne State University

<sup>2</sup>Iowa State University

<sup>3</sup>The University of Texas at Dallas

## Abstract

Dynamic voltage and frequency scaling (DVFS) and task-to-core allocation are critical for thermal management and balancing energy and performance in embedded systems. Existing approaches either rely on utilization-based heuristics that overlook stall times, or require extensive offline profiling for table generation, preventing runtime adaptation. Building upon hierarchical multi-agent scheduling, we contribute model-based reinforcement learning with accurate environment models that predict thermal dynamics and performance states, enabling synthetic training data generation and converging 20× faster than model-free methods. We introduce Large Language Model (LLM)-based semantic feature extraction that characterizes OpenMP programs through code-level features without execution, enabling zero-shot deployment for new workloads in under 5 seconds without workload-specific profiling. Two collaborative agents decompose the exponential action space, achieving 358ms latency for subsequent decisions. Experiments on Barcelona OpenMP Tasks Suite (BOTS) and PolybenchC benchmarks across NVIDIA Jetson TX2, Jetson Orin NX, RubikPi, and Intel Core i7 demonstrate 7.09× better energy efficiency, 4.0× better makespan, and 358ms decision latency compared to existing power management techniques.

## 1 Introduction

Energy-efficient embedded systems are limited by computational resources and are widely deployed in IoT devices, wearable electronics, and autonomous vehicles. In these systems, managing the thermal dynamics prevents thermal overheating, ensures system reliability, and avoids non-uniform aging due to uneven workload distribution among the cores [9, 18]. However, the available thermal-aware energy-efficient methods proposed for embedded systems lack scalability to many cores and adaptability to different platforms, especially in dynamic and resource-constrained environments, and often incur prohibitive computational overhead.

Dynamic Voltage and Frequency Scaling (DVFS) allows for runtime adjustment of voltage and frequency levels, balancing temperature and performance. Besides, an intelligent task migration and load balancing based on the operating system kernel helps redistribute computational tasks to avoid localized thermal hotspots. However, existing open-loop governors often prove inadequate in addressing the per-core frequency adjustments based on thermal behavior within embedded environments [18]. A feedback control technique can augment these methods by proactively tracking the temperature fluctuations and limiting the impact of thermal escalation [47, 40]. Various feedback-based algorithms based on meta-heuristics, integer programming, and machine learning have been proposed [73, 70, 81, 27, 35, 37, 28], but these approaches lack application-agnostic or computationally efficient structures for adaptation in real-time systems.

Given the complexity of embedded systems, the cost-intensive nature of collecting real-world data adds to the challenges of task and processor profiling. This complexity frequently leads to unpredictable execution time estimates, aggravated by limited hardware feedback mechanisms within these systems.

These challenges can significantly hinder efficient core allocation, affecting overall performance and energy efficiency. Consequently, existing task scheduling strategies mostly prioritize workload demand or only utilization metrics over temperature and system-related considerations. This trend is discernible in Linux kernel governors [9] and recently formulated policies [37, 28, 40]. As a result, these strategies often overlook detailed insights provided by system profilers during task execution [3] and allocate resource-intensive tasks to hot cores, which are more sensitive to temperature elevations. State-of-the-art heuristic approaches like the precise scheduler [7] achieve near-optimal energy efficiency for static frequency assignment through exhaustive offline profiling across all configurations, but require 8 to 12 hours of table generation per benchmark (e.g., profiling a 1 to 5 second task across all core-frequency combinations with multiple repetitions), preventing runtime adaptation. Their static nature limits adaptability to thermal variations and workload phase changes.

Model-based reinforcement learning (RL) uses a predictive model to simulate future states and make informed decisions, enhancing the adaptability and efficiency of embedded systems. Our approach focuses on average-case performance optimization for soft real-time and best-effort workloads, complementing (rather than replacing) hard real-time schedulers that provide formal Worst-Case Execution Time (WCET) guarantees. The environment model combined with Large Language Model (LLM)-extracted semantic features enables zero-shot deployment: RL agents train using synthetic data without profiling samples from the target platform, eliminating sample collection overhead. Model-based approaches enable low-latency decision-making. First decisions on new benchmarks require 3.5-8.0s including one-time LLM feature extraction, while subsequent decisions achieve 358ms (8,300 $\times$  faster than exhaustive profiling).

This paper introduces a thermal- and performance-aware model-based Multi-Agent Reinforcement Learning (MARL) approach for embedded systems with minimal real-data requirements. These MARL techniques enable collaborative decision-making among multiple agents to optimize system performance while considering thermal constraints [31]. The key objectives of our work are threefold: first, to develop a thermal-aware modeling framework that captures the thermal dynamics of embedded systems under varying workloads and environmental conditions; second, to integrate this modeling framework with zero-shot deployment techniques through an off-policy MARL approach to enable efficient adaptation to new platforms with zero profiling samples from target hardware; and third, to evaluate the effectiveness of the proposed approach in optimizing thermal management and system performance in real-world embedded systems, with emphasis on decision latency and makespan improvement of 4.0 $\times$  compared to exhaustive table-based and heuristic methods.

The proposed thermal-aware modeling approach augments the sample space by leveraging planning on trained models based on accurate data, contrary to previously proposed approaches based on direct Reinforcement Learning (RL) [64, 31, 42, 41]. We tune several multivariate regression model architectures and select computationally efficient models with low overhead and high accuracy. The proposed models outperform the accuracy of the state-of-the-art temperature modeling heuristics [23], achieving over 6 $\times$  better temperature prediction accuracy while maintaining model inference latencies under 5ms.

Through extensive experimentation and evaluation on representative embedded system platforms, we demonstrate the effectiveness of the proposed approach in achieving thermal awareness, performance optimization, and system reliability. Several low-energy methodologies are implemented including single-agent and multi-agent direct RL and model-based RL, to be compared with federated energy-aware scheduling [7] and Linux governors [9]. Our framework integrates runtime monitoring of temperature patterns using Linux in-kernel profiling and the Barcelona OpenMP Tasks Suite (BOTS) and PolybenchC for workload characterization [19]. By leveraging the capabilities of MARL, our approach offers a flexible and adaptive solution for zero-shot deployment of temperature-aware and energy-efficient scheduling on new embedded systems, enabling practical deployment in mobile and autonomous systems.

The key contributions of the paper are as follows:

- We integrate environment modeling into few-shot learning techniques through an off-policy MARL approach to enable efficient adaptation to new thermal scenarios with limited training data. The precise modeling framework reduces sample collection overhead, achieving 4.0 $\times$  better mean makespan compared to heuristic baselines while converging 20 $\times$  faster than model-free methods.

- We introduce LLM-based semantic feature extraction that characterizes OpenMP programs through 13 code-level features without execution. We evaluate three state-of-the-art LLMs (DeepSeek-V3, Claude Sonnet, GPT-4o), achieving up to 73.8% inter-model agreement, enabling zero-shot deployment to new platforms with one-time extraction cost of \$0.018 per program.
- We develop thermal-aware accurate modeling that captures thermal dynamics of embedded processors under varying workloads. The proposed regression models outperform state-of-the-art temperature prediction by a factor of over 6 in Mean Squared Error (MSE), with model inference latencies under 5ms.
- We evaluate the approach through extensive experiments using OpenMP benchmarks (BOTS and PolybenchC) on NVIDIA Jetson TX2, Jetson Orin NX, RubikPi, and Intel Core i7. Our model-based approach achieves 358ms inference latency for subsequent decisions and  $8,300\times$  faster first-decision latency than table-based profiling, while achieving  $7.09\times$  better energy efficiency than the Linux ondemand governor.

## 2 Related Work

Low-energy scheduling for multi-core platforms based on DVFS has received significant attention [73, 70, 69, 81, 72, 27, 14, 79, 13, 39, 77, 58, 59, 53, 26, 25, 34, 35, 71, 2, 1, 33]. The survey in [73] classifies all the low-energy parallel scheduling into energy-efficient, energy-aware, and energy-conscious styles, each based on heuristic, meta-heuristic, integer programming, and machine learning algorithms. Among these algorithms, only data-oriented machine learning, surveyed in [47], relies on historically collected data and addresses different application dynamics.

Due to the integration of DVFS in most commercial processors and their standard profiling and control, machine-learning algorithms are gaining significance in providing a dynamic environment [76, 29, 18, 82, 47, 57, 66, 75, 38, 56, 62, 65, 8]. The previous work [47] shows most of the machine learning algorithms for DVFS are based on model-free reinforcement learning, which implements a direct RL approach. None of this existing work addresses feature evaluation challenges or sample collection overhead.

Few-shot learning encompasses diverse techniques like transfer learning, model-based RL, inverse RL, imitation learning, and meta-learning, all applicable to DVFS due to its sampling demands [64, 31, 67, 42, 21, 16, 5, 68, 54]. While inverse RL infers reward functions from expert demonstrations [43], model-agnostic meta-learning adapts to new tasks with minimal data [20], and model-based RL approximates transition functions [41]. The works in [37, 28, 80, 78] utilize MARL, meta-state, transfer learning, and temporal dependencies on DVFS. The Q-learning algorithm in [76] performs clock gating on idle FPGA cycles rather than using DVFS as in [18]. None of these works address few shot learning and learning overhead in RL-based DVFS governors. The existing few-shot learning approaches also need an expert demonstration or cannot directly be applied in embedded systems.

Previous studies have investigated runtime sampling complexities in RL-based DVFS and proposed thermal predictive modeling for multi-core processors to predict thermal states [74, 10, 18, 23, 32, 40, 65]. The works in [37, 28] focus on temperature and utilization metrics and implement a command module on a separate neural network server. The predictive modeling in [40, 23] predicts the future thermal behavior of the multi-core processors given transient and ambient states. However, these RL training methods are computationally expensive on a single platform, and temperature models are inaccurate. Building upon hierarchical multi-agent DVFS [52], feature-aware statistical learning [51], and graph-driven performance modeling [50], this paper introduces computationally efficient and accurate modeling combined with flow-augmented few-shot learning techniques [49] and LLM-based semantic feature extraction, enabling a learning approach without requiring extra client-server interaction for frequency scaling.

Recent advances in Large Language Models (LLMs) have demonstrated remarkable capabilities in code understanding and performance prediction [15, 12, 45, 4, 17]. Laaber et al. [30] demonstrated that benchmark stability can be predicted using 58 statically-computed source code features without execution,

while Sanz et al. [55] applied neural networks to predict optimal thread counts for OpenMP regions. Recent work by Nichols et al. [44] investigated whether LLMs can predict GPU kernel performance characteristics using only source code, achieving up to 64% accuracy with reasoning-capable models in zero-shot settings. However, existing approaches for DVFS and task scheduling typically rely on runtime profiling or benchmark-specific identifiers, limiting their applicability to new platforms and workloads. This work bridges this gap by employing LLMs to extract semantic features from OpenMP programs that, combined with environment models, enable zero-shot deployment to new platforms without platform-specific profiling overhead.

### 3 Background and Motivation

Online learning to adjust DVFS and task-to-core allocation with a small number of hardware samples is a practical approach to control heat generation and energy consumption in multi-core platforms.

**DVFS.** The power consumption and thermal condition of a processor are proportional to the voltage and frequency, which also determine the workload performance. In our case, performance is measured as the makespan, i.e., the time taken from the start to the completion of the workload. The workloads considered here are BOTS benchmarks such as Strassen, FFT, and others, parallelized through the OpenMP API [19]. Existing Linux governors and energy-aware DVFS heuristics use utilization metrics to determine workload demand and adjust voltage and frequency [9, 22, 37]. For instance, the `ondemand` governor increases the frequency instantly when utilization crosses a threshold; similarly, the `conservative` governor incrementally increases frequency after exceeding the utilization threshold. The `schedutil` governor uses predictive utilization over a specific time window to predict future workload demand [9]. These governors achieve sub-millisecond decision latency but lack workload-aware optimization.

**Task-to-Core Allocation.** Due to the different performance characteristics of different types of cores and non-uniform memory access (NUMA), i.e., performance is relative to the proximity to memory, the makespan and power/energy consumption differ with respect to different core allocations. For example, in the NVIDIA Jetson TX2, the ARM Cortex-A57 cores correspond to cores 2, 3, 4, and 5, which are power-efficient cores, while the NVIDIA Denver cores (cores 0 and 1) are more suited for performance-critical tasks and are by default turned off for power efficiency. It is possible to allocate a set of cores and memory nodes through the `cpuset` feature of the Linux kernel. Additionally, CPU affinity, i.e., binding specific threads of execution to specific cores, helps reduce context switches and enhances performance in terms of makespan and energy efficiency. Intelligent allocation of cores to the input workload helps distribute processing, reducing the concentration of processing in a specific spot in the processor, thereby decreasing the thermal throttling possibility.

**Online Learning for DVFS and Task-to-Core Allocation.** The online learning approach for DVFS and task-to-core allocation is often based on RL using a Markov Decision Process (MDP) that depends on the previous state (observed multi-core platform performance data), the taken action (frequency scaling and task-to-core allocation), and observing the current state after applying this action. The objective in RL is to apply actions based on observed states that maximize the expected sum of future rewards with the defined reward function [6, 24]. In a direct RL approach, the learning algorithm is based on exploration and exploitation; exploration involves taking random actions, and exploitation refers to taking actions based on the policies trained through observing the previous and current states. This training continues for a time horizon until the learning algorithm converges. For example, with Q-learning, the states mapped to the actions are given values called Q-values, and convergence happens when the taken actions are optimized according to the defined reward function in terms of maximum accumulated rewards. RL methods using neural networks typically achieve inference latencies of 1-10 milliseconds on embedded platforms.

**Deep Q-learning and Enhanced D3QN.** The profiling data extracted from parallel workloads (e.g., BOTS benchmarks) is continuous, meaning the state space cannot be simply mapped to the action space through a Q-function in Q-learning. Deep Q-learning leverages neural networks to approximate these Q-values. Deep Q-learning provides sample efficiency by training through past experiences stored as

state-action pairs inside a replay buffer. To mitigate issues like overestimation of actions, the Q-function utilizes Dueling Deep Q-Networks (D3QN), i.e., decomposing the Q-function into a value function and an advantage function, where the value function gives a global value for each corresponding state and the advantage function evaluates the advantage of taking an action in the corresponding state. The Q-value is assigned to a corresponding state-action pair by taking an action based on the same deep Q-network with respect to the target, i.e., maximized future rewards. To make the action selection independent from the module that calculates the Q-value, a parallel Deep Q-network is designed, resulting in a double dueling deep Q-Network (D3QN). These strategies allow the Deep Q-Network to learn optimal configurations, such as adjusting CPU frequencies and allocating tasks to specific cores. As a result, the system can dynamically manage multi-core resources, achieving improved performance and energy efficiency through a stable and data-driven policy.

**Table-Based Heuristic Scheduling.** State-of-the-art energy-aware schedulers such as the precise scheduler [7] achieve near-optimal energy efficiency through exhaustive offline profiling, generating lookup tables by executing tasks across all frequency-core combinations. However, table generation requires extensive offline profiling (hours to days), and any workload change necessitates complete regeneration. While table lookup achieves sub-millisecond latency, the lack of runtime adaptability limits deployment in dynamic environments.

**Motivation on Model-Based MARL.** Model-based RL provides a more efficient, adaptable, and robust framework for optimizing DVFS and task-to-core allocation in multi-core systems, achieving fast convergence and low decision latency.

**Limitations of Utilization-Based DVFS.** Most of the available Linux kernel governors take CPU utilization to scale voltage and frequency. Utilization is defined as  $Utilization = T_{busy} / (T_{busy} + T_{idle})$ , where  $T_{busy}$  is the time the processor is active (including both execution and stall times), and  $T_{idle}$  is the idle time. The busy time  $T_{busy}$  comprises both *active* time ( $T_{active}$ ), when the processor is executing instructions, and *stall* time ( $T_{stall}$ ), when execution is delayed due to factors like branch mispredictions, context switching overhead, cache misses, etc. [22]. Stall time can account for more than 50% of a workload’s execution time [37], yet utilization-based DVFS does not differentiate between the active and stall times. Thus, the utilization-aware frequency scaling may result in a less effective solution to match the frequency to the actual demand of the workload.

**Challenges in Task-to-Core Allocation.** Due to the characteristics of different core types and different properties of tasks, the set and the number of cores to be allocated to the parallel workload should be carefully determined. Many modern processors support heterogeneous computing by combining cores with different characteristics to enhance power efficiency and performance capabilities. Moreover, many modern processors have non-uniform memory access (NUMA), i.e., cores have different proximity to memory locations, resulting in performance degradation for distant cores. Selecting the cores also affects thermal throttling; overloading nearby cores can stall workload execution and accelerate processor aging. Selection of the number of cores to be allocated to the parallel tasks is also important.

For example, in an OpenMP workload, where each thread of execution represents a core, *tied* tasks should be restricted to execute on the allocated core. In contrast, *untied* tasks can migrate to other cores. Unpredictable execution time of a tied task, caused by branch misses, can lead to overall unpredictability in the workload’s makespan. This introduces timing unpredictability, impacting the overall makespan and energy/power consumption. As a result, increasing the number of allocated cores in this case increases unpredictability and does not lead to improved performance [3]. In sum, to make informed decisions on

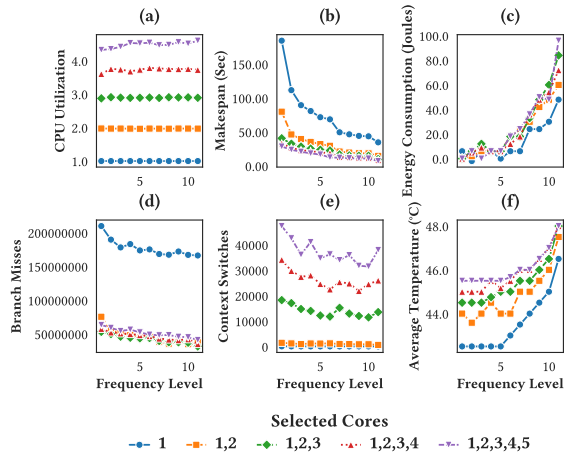


Figure 1: Performance metrics for FFT on Jetson TX2 across frequency/core configurations.

task-to-core allocation, observation variables such as branch misses, cache misses, context switches, and each core’s temperature should be given appropriate attention.

Figure 1 highlights observation features at different frequency levels and core counts on NVIDIA Jetson TX2 running FFT. The frequency has 12 levels (0=lowest, 11=highest). CPU utilization increases with cores but shows minimal frequency impact. Makespan reduces with higher frequency but shows diminishing returns beyond two cores. Energy consumption increases sharply with frequency and core count. Branch misses exhibit a large gap between single and multiple cores but remain frequency-independent. Context switches rise with cores, indicating allocation inefficiency. Temperature increases with frequency and core count, risking thermal throttling.

### **Environment Modeling and Multi-Agent RL.**

To effectively address both DVFS and task-to-core allocation while enhancing sample efficiency, we develop an accurate environment model and employ a multi-agent reinforcement learning (RL) framework. An accurate environment model captures the system’s characteristics, including hardware architecture, workload behavior, and their interactions, enabling low-cost synthetic sample generation for *few-shot* learning. By modeling the environment and incorporating factors such as branch misses, cache misses, and context switches, more precise and efficient strategies for energy optimization can be devised.

Implementing a multi-agent RL approach allows multiple agents to focus on different optimization tasks, such as frequency scaling and core allocation, each with potentially different reward definitions tailored to their specific goals. This specialization enhances the generalizability and effectiveness of the online learning process, as agents can learn optimal strategies in parallel and adapt to changing conditions more quickly. Together, environment modeling and multi-agent RL provide a robust framework for dynamically managing multi-core resources, leading to improved performance and energy efficiency. Model-based MARL addresses the trade-off between decision quality and decision latency: while table-based methods achieve optimal energy efficiency, their offline profiling requires hours. In contrast, model-based RL achieves 20× faster convergence with inference latencies under 10ms, which is orders of magnitude faster than table regeneration, enabling practical deployment with energy accuracy within 4% of optimal.

**LLM-Based Workload Profiling.** Traditional workload characterization relies on either exhaustive runtime profiling (8-12 hours per platform) or syntactic static analysis that captures code structure but not semantic meaning. Recent Large Language Models (LLMs) such as GPT-4 [45], Claude [4], and DeepSeek [17] enable zero-shot semantic feature extraction from source code without execution. LLMs can infer algorithmic complexity, memory access patterns, parallelization characteristics, and synchronization overhead by analyzing code semantics. This enables performance prediction for unseen workloads and cross-platform transfer learning, as semantic features (e.g.,  $O(n^2)$  complexity, unit-stride access) remain platform-agnostic. We extract 13 semantic features across memory, algorithmic, and parallelization dimensions to complement hardware performance counters, achieving MAPE under 15% for zero-shot predictions.

## **4 Design of Model-Based Thermal- and Energy-Aware MARL**

The proposed framework enables few-shot learning by generating synthetic data for agents that manage frequency scaling and task-to-core allocation on multi-core platforms, achieving low decision latency and fast convergence compared to exhaustive table-based approaches.

### **4.1 Design of MARL**

Optimizing both DVFS and task-to-core allocation through RL is impractical due to high-dimensional action space and we need to break actions through introduction of multiple agents with separate goal definitions, which also reduces inference latency by decomposing complex decisions.

**High-Dimension Action Space.** The goal of the thermal- and energy-aware parallel scheduling in this paper is to dynamically adjust the voltage and frequency of the subset of the high priority cores based

on cores and parallel workload characteristics. Regarding a naive single-agent implementation, the action space for this environment would be exponentially related to the frequency levels, the number of cores, and the combination of cores altogether, as shown in the following observation.

**Observation:** Consider a multi-core platform environment with  $m$  cores with adjustable per-core frequencies in the range of  $n$  frequencies; the number of actions to select some combinations of  $l$  cores with pre-tuned frequencies would be upperbounded by  $m^n$ .

To construct the action space,  $l$  cores must be selected from a total of  $m$  cores, which can be achieved using a combination formula like  $\binom{m}{l}$ . Suppose we only assign one frequency to all cores in the combination of cores in the range of  $n$  frequency conditions. In that case, the number of possible actions can be obtained by summing over the different numbers of core choices using a binomial coefficient. Thus, the total number of actions, disregarding frequency, is given by  $\sum_{i=1}^m \binom{m}{i}$ , which can be approximated to  $2^m$  actions. However, suppose we include each core in the selected combination of cores to be associated with a frequency in the range of  $n$  frequencies; the previous formula changes to  $\sum_{i=1}^m \binom{m}{i} 2^n$  that can be upper-bounded by  $m^n$ . For table-based approaches like the precise scheduler [7], this exponential action space necessitates exhaustive offline profiling across all configurations, requiring hours to days of execution time.

To address this challenge, we adopt a collaborative hierarchical MARL approach that decomposes the exponential action space into lower-dimensional sub-problems handled by separate agents implemented as Double Deep Q-Networks (D3QN). The final action is a combination of each agent’s decision. We use two primary agents:

- *Profiler Agent:* Assesses workload performance to minimize energy consumption and makespan by determining the appropriate number of cores and the operating frequency
- *Temperature Agent:* Prioritizes cores based on their temperature to prevent heat concentration.

In the hierarchical decomposition, the action that assigns frequency to a core is called ( $a_{freq}$ ) and the input energy consumption state ( $s_{energy}$ ) determines Q-value  $Q(a_{freq}, s_{energy})$ , while the action that assigns the number of cores is called ( $a_{cores}$ ) based on workload performance state ( $s_{workload}$ ) that determines Q-value  $Q(a_{cores}, s_{workload})$ . To decrease the computational overhead, these two agents are combined resulting in profiler action  $a_{profiler} : \{a_{cores}, a_{freq}\}$  from the profiler state  $s_{profiler} : \{s_{energy}, s_{workload}\}$ . Priority assignment action ( $a_{temp}$ ) is based on the core thermal state ( $s_{temp}$ ), determining Q-value  $Q(a_{temp}, s_{temp})$ . Assigning a frequency from  $n$  frequency levels to  $m$  cores results in  $m \times n$  possible actions. Selecting from  $m$  possible number of cores results in  $m$  choices, and for priority selection, we have choices from  $m \times m$  possible actions. Introducing sequential action selection in MARL reduces this to  $m \times m + m \times n + m$  possible choices, enabling inference latency under 10ms on embedded platforms.

**Reward Function Definition.** The reward functions for the Profiler and Temperature agents are designed to guide the system toward optimal performance and energy efficiency. Unlike previous studies [37, 28], which rely on CPU utilization and frame rate as target metrics, our approach focuses on makespan and energy consumption of suboptimal conditions defined by performance and powersave linux governors to provide a more accurate assessment of workload performance. This shift addresses the limitations of utilization metrics (defined as  $utilization = t_{busy} / (t_{busy} + t_{idle})$ ), which can be misleading by overlooking stall times. Additionally, to prevent thermal throttling, we enforce a temperature limit of 50°C based on the thermal throttling threshold of the Jetson TX2.

For the Temperature agent, we employ a linear reward function designed to maintain core temperatures below the 50°C threshold. Specifically, for each core, if its temperature exceeds 50°C, the reward is set to  $-1$ , penalizing actions that lead to overheating. Conversely, if the temperature remains below the threshold, the reward is calculated as the difference between 50°C and the current temperature of the core. Mathematically, the reward for core  $i$  is defined as:

$$r_{temp}^i = \begin{cases} -1 & \text{if } temp_i > 50^\circ\text{C}, \\ 50 - temp_i & \text{otherwise.} \end{cases}$$

The overall temperature reward is then computed as the average of these individual rewards across all  $m$  cores:

$$r_{\text{temp}} = \frac{1}{m} \sum_{i=1}^m r_{\text{temp}}^i.$$

This structure incentivizes the agent to keep all cores cool, thereby preventing thermal throttling and ensuring sustained performance.

In contrast, the Profiler agent utilizes an exponential reward function to balance energy consumption and makespan. The reward is determined based on how closely the system’s performance metrics approach their target values. We define two parameters: the *threshold factor*  $c_{\text{th}} = 0.3$  controls the penalization boundary relative to baseline performance, and the *steepness factor*  $c_{\text{st}} = 0.5$  controls how rapidly rewards decay as metrics deviate from targets. Specifically, if the agent total energy consumption ( $E_A$ ) exceeds the target set by the powersave governor ( $E_{\text{Psav}}$ ) or if the agent makespan ( $\text{makespan}_A$ ) surpasses the target set by the performance governor ( $\text{makespan}_{\text{Perf}}$ ) by a factor of  $c_{\text{th}}$ , the reward is set to  $-1$ , discouraging inefficient configurations. Otherwise, the reward increases exponentially as energy consumption and makespan approach their targets, defined as:

$$r_{\text{energy}} = e^{-c_{\text{st}} \times \frac{E_A - E_{\text{Psav}}}{c_{\text{th}}}} \times 2 - 1,$$

$$r_{\text{makespan}} = e^{-c_{\text{st}} \times \frac{\text{makespan}_A - \text{makespan}_{\text{Perf}}}{c_{\text{th}}}} \times 2 - 1.$$

The final profiler reward is the average of the energy consumption and makespan rewards:

$$r_{\text{profiler}} = \frac{r_{\text{energy}} + r_{\text{makespan}}}{2}.$$

Here,  $E_{\text{total}}$  represents the total energy consumption, and makespan denotes the workload completion time. The parameters  $c_{\text{th}}$  and  $c_{\text{st}}$  control the threshold for penalization and the steepness of the exponential increase, respectively. By adjusting these parameters, we can prioritize either energy efficiency or makespan based on the specific optimization objectives in each agent. These distinct reward functions guide the profiler agent to optimize for energy and makespan while the temperature agent maintains thermal constraints.

**Complexity Analysis of Agents.** Each agent in the proposed energy-aware hierarchical MARL scheduler requires individual training to assign meaningful weights to observations for reward evaluation, increasing computational complexity. However, this complexity is justified by the improved sample efficiency achieved through the off-policy Q-learning method. We employ the D3QN to address this, which provides practical agent training. Once trained, neural network inference is fast (sub-10ms), enabling practical deployment. In case of model inference failure or anomalous predictions, the system gracefully degrades to the Linux ondemand governor, which represents our baseline and ensures continued operation without service interruption.

Let  $N_{\text{agent}}$  represent the number of agents,  $N_{\text{hidden}}$  be the number of hidden layer neurons,  $N_{\text{state}}$  be the dimension of the input observations, and  $N_{\text{actions}}$  be the dimension of the output actions. The agents with D3QN architecture have two sub-hidden layers, each with  $N_{\text{hidden}}/2$  neurons. The first layer calculates advantages, resulting in an output layer of size equal to the number of actions  $N_{\text{actions}}$ . The second layer calculates values and has a single neuron in its output layer.

The total number of network parameters for a single agent is:

$$\begin{aligned} \text{Parameters} = & 2 \times ((N_{\text{state}} \times N_{\text{hidden}} + N_{\text{hidden}}) \\ & + (N_{\text{hidden}} \times N_{\text{actions}} + N_{\text{actions}}) \\ & + (N_{\text{hidden}} \times 1 + 1)) \end{aligned}$$

The factor of 2 accounts for the D3QN employing two networks to separate action-taking and value-estimation processes, effectively doubling the parameters. Assuming all agents have similar action and

observation dimensions, the total number of parameters in the hierarchical MARL can be estimated by multiplying the parameters per agent by the total number of agents:

$$\text{Total Parameters} = N_{\text{agent}} \times \text{Parameters}$$

To enhance the model’s efficiency regarding computational complexity, it is essential to optimize the number of hidden neurons  $N_{\text{hidden}}$  and carefully balance the number of agents  $N_{\text{agent}}$ . Techniques such as parameter sharing among agents, pruning less significant neurons, and employing more efficient network architectures can significantly reduce the total number of parameters. Additionally, leveraging hardware accelerations like GPUs or specialized AI processors can mitigate the computational overhead, ensuring scalable and efficient training of the hierarchical MARL system. In this implementation, we separate the client that is the targeted Jetson TX2 as platform from the server where the online learning algorithm is implemented to deal with computational complexity. This client-server architecture amortizes training cost offline while maintaining lightweight inference on the embedded platform, achieving decision latency orders of magnitude faster than table regeneration for any configuration changes.

## 4.2 Environment Design and Modeling

The model of the environment consists of a model for temperature agent and a model for profiler agent implemented and verified through a variety of regression algorithms, selected for both accuracy and low inference latency.

**Proposed Model-Based Hierarchical MARL Approach.** In a model-free RL context, agents interact directly with the environment and train based on the real data. In contrast, model-based RL involves simulation data along with the real data extracted from the environment. Inference from the dynamic model (planning) speeds up agent training and hyperparameter tuning, requiring fewer samples for convergence than only gathering real data. As shown in Figure 2, agents are trained either with environment observations or the dynamic model. This model-based approach achieves significantly faster convergence compared to model-free methods and avoids the extensive offline profiling required by table-based approaches.

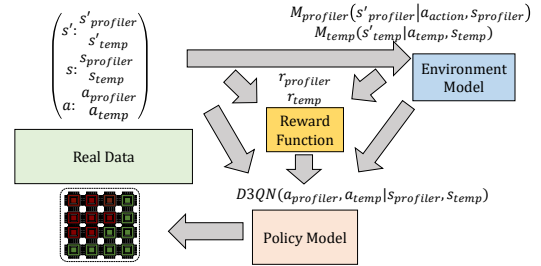


Figure 2: The simplified design of model-based RL for temperature- and energy-aware core allocation for multi-core processors.

The proposed model-based hierarchical MARL approach is inspired by the Dyna-Q algorithm [48], as shown in Algorithm 1. Dyna-Q is particularly well-suited for this application because it effectively integrates learning and planning, allowing agents to leverage both real and simulated experiences. This integration enhances sample efficiency, which is crucial in complex multi-agent environments like energy-aware scheduling in multi-core processors where real-world interactions can be time-consuming and resource-intensive. By utilizing a dynamic model to generate simulated experiences, the approach accelerates training convergence and reduces the reliance on extensive real-world data collection. Additionally, Dyna-Q’s framework supports scalability and robustness, enabling the system to adapt to varying workload patterns and efficiently manage multiple agents operating at different levels of abstraction. Compared to exhaustive table generation, this approach completes training in minutes rather than hours while enabling runtime adaptation.

The Algorithm 1 begins by initializing separate replay memories for both the profiler and temperature agents, along with their respective dynamic models and value functions. Parameters such as threshold  $\zeta$  for planning steps and batch size  $\beta$  for training are also set. The training process is divided into multiple episodes, each starting with the initialization of the profiler and temperature states. Within each episode, the algorithm enters a loop that continues until a termination condition is met for either agent. In the **Direct RL** phase, each agent selects an action based on its current policy derived from its respective

---

**Algorithm 1** Model-Based Hierarchical Multi-Agent RL

---

```
1: Initialize:
2:   Replay memories  $B_{\text{profiler}}$  and  $B'_{\text{profiler}}$  for the profiler agent
3:   Replay memories  $B_{\text{temp}}$  and  $B'_{\text{temp}}$  for the thermal agent
4:   Dynamic model  $M_{\text{profiler}}$  for the profiler agent
5:   Value functions  $D3QN_{\text{profiler}}$  and  $D3QN_{\text{temp}}$ 
6:   Parameters: planning threshold  $\zeta$ , batch size  $\beta$ 
7: for each episode = 1 to  $H$  do
8:   Initialize states  $s_{\text{profiler}}$  and  $s_{\text{temp}}$ 
9:   while not done do
10:    Direct RL:
11:    Select action  $a_{\text{profiler}}$  using  $D3QN_{\text{profiler}}$ 
12:    Select action  $a_{\text{temp}}$  using  $D3QN_{\text{temp}}$ 
13:    Execute actions  $a_{\text{profiler}}$  and  $a_{\text{temp}}$  in the environment
14:    Observe next states  $s'_{\text{profiler}}, s'_{\text{temp}}$ 
15:    Observe rewards  $r_{\text{profiler}}, r_{\text{temp}}$ , and done flags  $d_{\text{profiler}}, d_{\text{temp}}$ 
16:    Store  $(s_{\text{profiler}}, a_{\text{profiler}}, r_{\text{profiler}}, s'_{\text{profiler}})$  in  $B_{\text{profiler}}$ 
17:    Store  $(s_{\text{temp}}, a_{\text{temp}}, r_{\text{temp}}, s'_{\text{temp}})$  in  $B_{\text{temp}}$ 
18:    if Model training condition is met then
19:      Train  $M_{\text{profiler}}$  using samples from  $B_{\text{profiler}}$ 
20:    end if
21:    Planning:
22:    for each planning step = 1 to  $\zeta$  do
23:      Generate action  $a'_{\text{profiler}}$  (randomly or from policy)
24:      Predict  $s''_{\text{profiler}}, r'_{\text{profiler}}$  using  $M_{\text{profiler}}$ 
25:      Derive  $s''_{\text{temp}}, r'_{\text{temp}}$  from  $s''_{\text{profiler}}$ 
26:      Store  $(s_{\text{profiler}}, a'_{\text{profiler}}, r'_{\text{profiler}}, s''_{\text{profiler}})$  in  $B'_{\text{profiler}}$ 
27:      Store  $(s_{\text{temp}}, a_{\text{temp}}, r'_{\text{temp}}, s''_{\text{temp}})$  in  $B'_{\text{temp}}$ 
28:    end for
29:    if Agent training condition is met then
30:      Sample minibatch from  $B_{\text{profiler}}$  and  $B'_{\text{profiler}}$ 
31:      Train  $D3QN_{\text{profiler}}$  with the minibatch
32:      Sample minibatch from  $B_{\text{temp}}$  and  $B'_{\text{temp}}$ 
33:      Train  $D3QN_{\text{temp}}$  with the minibatch
34:    end if
35:    Update  $s_{\text{profiler}} \leftarrow s'_{\text{profiler}}, s_{\text{temp}} \leftarrow s'_{\text{temp}}$ 
36:    Check termination: If  $d_{\text{profiler}}$  or  $d_{\text{temp}}$  is True, exit loop
37:  end while
38: end for
```

---

Q-value function ( $D3QN_{\text{profiler}}$  and  $D3QN_{\text{temp}}$ ), executes the action in the environment, and observes the resulting next state, reward, and done flag. These transitions are stored in their corresponding real replay memories ( $B_{\text{profiler}}$  and  $B_{\text{temp}}$ ). If the conditions for training the dynamic models are satisfied, only the profiler’s model  $M_{\text{profiler}}$  is trained using samples from  $B_{\text{profiler}}$ . The temperature agent does not have a separate dynamic model.

Following the **Planning** phase, the algorithm generates a predefined number of simulated transitions ( $\zeta$  steps) for each agent. These simulated transitions are generated using the profiler’s dynamic model  $M_{\text{profiler}}$ , and the thermal synthetic data is derived from the profiler’s predictions. For each planning step, actions are generated (either randomly or based on the current policy), and the dynamic models predict the subsequent states and rewards. These simulated transitions are stored in the simulated replay memories ( $B'_{\text{profiler}}$  and  $B'_{\text{temp}}$ ). The profiler’s simulated transitions are stored in  $B'_{\text{profiler}}$ , while the thermal synthetic transitions are inferred and stored in  $B'_{\text{temp}}$  based on the profiler’s predictions. If the conditions to train the agents are met, minibatches are sampled from both the real and simulated replay memories, and the Q-value functions ( $D3QN_{\text{profiler}}$  and  $D3QN_{\text{temp}}$ ) are trained using these samples. The current states are then updated to the next states, and the loop checks whether the episode should terminate based on the done flags. This iterative process ensures that both agents benefit from real and simulated experiences, enhancing their learning efficiency and adaptability in managing energy consumption and thermal states within multi-core processors.

By adopting the Dyna-Q-inspired framework, the proposed hierarchical MARL approach achieves a balance between efficient learning and practical scalability. This ensures that the system can effectively

manage energy consumption and thermal states in multi-core processors while maintaining computational efficiency and adaptability to dynamic workloads. Optimizing the training conditions and leveraging both real and simulated data streams allows the model to converge faster and operate reliably in complex, real-world scenarios.

**Different Environment Models and their Computational Complexity.** To determine the most efficient architecture for the environment model, we evaluate five regression models for predicting profiler states ( $s'_{\text{profiler}}$ ) and temperature states ( $s'_{\text{temp}}$ ), where inputs comprise the concatenated state-action vectors ( $N_{\text{input}} = N_{\text{state}} + N_{\text{action}}$ ). The models range in complexity: a Simple Fully Connected Network (FCN) with one hidden layer of  $N_{\text{hidden}}$  neurons yields  $O(N_{\text{input}} \cdot N_{\text{hidden}} + N_{\text{hidden}} \cdot N'_{\text{state}})$  parameters with 2–5ms inference latency; a one-dimensional Convolutional Neural Network (CNN) with kernel size  $K$  and  $C_{\text{out}}$  output channels requires  $O(K \cdot N_{\text{input}} \cdot C_{\text{out}})$  parameters at 4–8ms latency; a Recurrent Neural Network (RNN) with  $N_{\text{hidden}}$  neurons adds recurrent connections scaling as  $O(N_{\text{hidden}}^2)$ ; a Long Short-Term Memory (LSTM) network triples the RNN parameter count due to its forget, input, and output gates, with proportionally higher latency; and an Attention-Based Network [63] with  $H$  heads and hidden dimension  $N_{\text{hidden}}$  scales as  $O((N_{\text{input}} + 2)^2 \cdot H \cdot N_{\text{hidden}})$ , offering superior accuracy at higher computational cost. In practice, FCN and Conv1D achieve over  $6\times$  better temperature prediction accuracy than prior work [23] while maintaining inference latencies under 5ms on Jetson TX2, enabling efficient planning with synthetic data generation. Table 2 compares all models.

### 4.3 Cross-Platform Model Transfer and Adaptation

A key advantage of our learned environment model is its ability to transfer across platforms without requiring exhaustive re-profiling. Unlike table-based approaches that must regenerate all lookup entries when deployed on new hardware, our neural network models encode generalizable relationships between workload characteristics, system configuration, and performance outcomes. This section describes our transfer learning methodology for cross-platform deployment.

**Transfer Learning Methodology.** We employ a two-stage transfer learning approach:

**Stage 1: Zero-Shot Transfer.** The environment model trained on the source platform (Jetson TX2) is directly applied to the target platform without any modification. This provides a baseline for transfer quality and works because workload characteristics, including algorithmic complexity, memory access patterns, and parallelism, are ISA-agnostic. Furthermore, relative performance trends such as frequency scaling impact and core allocation effects generalize across platforms, while neural network representations capture underlying physical relationships that remain consistent across hardware implementations.

**Stage 2: Few-Shot Fine-Tuning.** The transferred model is refined using a small number of samples (5, 10, or 50) collected from the target platform. This fine-tuning process adapts frequency scaling coefficients to platform-specific P-states, calibrates thermal prediction to accommodate different cooling solutions, and adjusts energy consumption estimates to match platform TDP characteristics.

**Feature Classification for Transfer.** We categorize features based on their transferability:

**Platform-Agnostic Features (high transferability):** These features exhibit strong generalization across different hardware architectures. They include algorithmic complexity and computational patterns, memory access locality and data structure characteristics, parallelism structure and task dependencies, as well as branch prediction patterns and control flow complexity.

**Platform-Specific Features (require adaptation):** These features require calibration when transferring between platforms. They encompass absolute frequency values (normalized to [0,1] range), per-core temperature readings (normalized to thermal headroom), energy consumption (normalized to platform TDP), and core count and heterogeneity configuration.

By normalizing platform-specific features relative to each platform’s operating range, we maximize the transferable knowledge while enabling platform-specific calibration through fine-tuning.

**Transfer Learning Results.** The cross-platform transfer learning results are presented in Section 5 (Table 3). Our experiments evaluate zero-shot transfer from Jetson TX2 to Orin NX and RubikPi platforms, demonstrating the domain shift effects when deploying learned models across different

embedded architectures. The source platform achieves 10.9% MAPE (Mean Absolute Percentage Error), while zero-shot transfer shows 64.5% and 73.2% MAPE for Orin NX and RubikPi respectively, reflecting significant architectural differences between platforms.

#### Comparison with Table-Based Approaches.

The transfer learning capability provides a fundamental advantage over table-based schedulers. While deploying a table-based scheduler on a new platform requires  $T_{table} = m \times k \times |\Gamma| \times \rho \times \bar{t}$  profiling time, where  $m$  is the number of cores,  $k$  is the number of frequency levels,  $|\Gamma|$  is the cardinality of the task set,  $\rho$  is the number of repetitions, and  $\bar{t}$  is the average execution time (typically 8 to 12 hours), our approach achieves 5.7ms RL inference latency, representing over 5 million times faster adaptation capability for practical deployment in heterogeneous fleet environments.

## 4.4 LLM-Based Semantic Feature Extraction

Traditional performance prediction models for DVFS scheduling rely on benchmark identifiers to distinguish workloads, creating a fundamental limitation: they cannot generalize to programs absent from the training set. When a new application arrives, exhaustive profiling across all frequency-core configurations must be repeated. This process requires 8 to 12 hours per program on our target platforms, where each benchmark execution takes 1 to 5 seconds. We address this limitation by replacing opaque benchmark identifiers with interpretable semantic features extracted directly from source code, enabling zero-shot prediction for previously unseen workloads.

**Motivation: From Syntax to Semantics.** The challenge of workload characterization without execution traces requires distinguishing between what code *contains* versus how it *behaves*. Traditional static analysis tools such as Tree-sitter [60] and compiler front-ends excel at extracting syntactic properties, such as counting loops, identifying OpenMP pragmas, and measuring code complexity metrics. However, these tools fundamentally cannot infer semantic properties that determine runtime behavior.

Consider the limitations of purely syntactic analysis. A parser detecting three nested loops cannot determine whether they implement  $O(n^3)$  matrix multiplication or  $O(n^{2.807})$  Strassen’s algorithm; the syntactic structure appears identical despite dramatically different scaling behavior. Similarly, array indexing syntax `A[i][j]` reveals nothing about whether memory accesses exhibit unit-stride patterns amenable to hardware prefetching or scattered patterns that thrash the cache hierarchy. These semantic judgments require understanding algorithmic intent rather than merely parsing code structure.

Large language models trained on extensive code corpora offer a compelling solution. Unlike rule-based analyzers, LLMs can recognize algorithmic patterns, reason about data flow dependencies, and assess parallelization characteristics through learned representations of programming concepts. We leverage this capability to extract 13 semantic features that complement the 17 syntactic features obtained through traditional static analysis.

**Two-Stage Feature Extraction Pipeline.** Our feature extraction operates in two complementary stages. The first stage employs Tree-sitter to extract syntactic features capturing the structural composition of OpenMP programs: control flow metrics such as loop depth and nesting complexity, OpenMP directive counts including parallel regions and task constructs, synchronization primitives such as critical sections and atomic operations, and variable scope classifications distinguishing shared, private, and reduction variables. These 17 features provide a syntactic fingerprint of code structure but cannot distinguish semantically different algorithms with similar structural properties.

The second stage queries large language models to extract semantic features requiring deeper code understanding. We employ three state-of-the-art models, namely DeepSeek-V3 [17], Claude Sonnet [4], and GPT-4o [45], using zero-shot prompts that request structured JSON responses. The term “zero-shot” applies at three distinct levels in our methodology. At the prompting level, we provide no in-context examples to the LLM, avoiding bias toward specific patterns while reducing token costs. At the prediction level, our trained model generalizes to entirely new programs without retraining. Most importantly, at the deployment level, the environment model combined with LLM-extracted features enables zero-shot transfer to new platforms: the RL agent can be trained using synthetic data generated by the environment

model without requiring any profiling samples from the target hardware. This is the key distinction from prior transfer learning approaches that still require sample collection on target platforms.

The semantic features span three categories reflecting distinct aspects of workload behavior. Memory access characteristics capture spatial and temporal locality, cache utilization patterns, and NUMA sensitivity. These are properties that determine memory subsystem efficiency at different frequency settings. Algorithmic characteristics encode computational complexity, dominant operation types, and vectorization potential, distinguishing compute-bound workloads that benefit from higher frequencies from memory-bound workloads where frequency scaling yields diminishing returns. Parallelization characteristics assess data dependencies, load balance properties, synchronization overhead, and scalability bottlenecks, informing core allocation decisions in the hierarchical scheduling framework.

**Multi-Model Agreement and Reliability.** Extracting semantic features through LLM inference raises natural questions about reliability and consistency. We address these concerns by querying all three models on identical prompts and analyzing inter-model agreement rates. Table 1 presents pairwise and unanimous agreement percentages across the 42 benchmarks in our evaluation suite.

The agreement analysis reveals a meaningful hierarchy of feature reliability. High-consensus features such as dominant operation (73.8% unanimous agreement) and algorithmic complexity (59.5%) reflect well-defined code patterns where models reach consistent conclusions. These features provide robust signals for distinguishing compute-bound from memory-bound workloads and predicting frequency scaling behavior. Conversely, low-agreement features including false sharing risk (14.3%) and cache behavior patterns (16.7%) involve subtle

Table 1: Inter-Model Agreement Rates for Semantic Features (%)

Feature	DS-CL <sup>a</sup>	DS-GPT <sup>b</sup>	CL-GPT <sup>c</sup>	All 3
dominant_operation	83.3	88.1	76.2	<b>73.8</b>
algorithmic_complexity	69.0	78.6	66.7	59.5
temporal_locality	66.7	81.0	47.6	47.6
load_balance	40.5	88.1	47.6	38.1
parallelization_overhead	45.2	59.5	64.3	38.1
vectorization_potential	47.6	69.0	50.0	35.7
spatial_locality	59.5	52.4	50.0	31.0
memory_access_pattern	61.9	33.3	28.6	21.4
data_dependency_type	38.1	42.9	50.0	21.4
cache_behavior_pattern	69.0	33.3	28.6	16.7
false_sharing_risk	23.8	50.0	40.5	<b>14.3</b>

<sup>a</sup> DS-CL: DeepSeek-V3 vs. Claude Sonnet agreement.

<sup>b</sup> DS-GPT: DeepSeek-V3 vs. GPT-4o agreement.

<sup>c</sup> CL-GPT: Claude Sonnet vs. GPT-4o agreement.

judgments where reasonable disagreement is expected even among human experts. Rather than discarding these features, our gradient boosting predictor learns appropriate importance weights during training, automatically down-weighting unreliable signals while leveraging consistent features more heavily.

**Cost-Effective Zero-Shot Prediction.** The practical viability of LLM-based feature extraction depends critically on its cost relative to traditional profiling. Our analysis shows favorable cost trade-offs. Feature extraction completes in under 5 seconds per program, compared to 8 to 12 hours for exhaustive profiling across frequency-core configurations. The monetary cost ranges from \$0.0015 per program using DeepSeek-V3 alone to \$0.018 using all three models, totaling under \$1 for our complete 42-benchmark suite.

Crucially, feature extraction is a one-time operation. Once extracted, semantic features are cached and reused for unlimited subsequent predictions across any number of target platforms without additional API calls. This approach significantly reduces costs: profiling 1,000 programs across all configurations would require approximately \$400,000 in labor costs assuming \$50/hour and 8 hours per benchmark, while LLM extraction costs \$18 total using all three models or merely \$1.50 using only DeepSeek-V3. The four-order-of-magnitude cost reduction enables practical deployment of zero-shot prediction in scenarios where traditional profiling is economically infeasible.

In conclusion, the proposed model-based hierarchical MARL approach effectively combines direct reinforcement learning and planning using dynamic models to improve sample efficiency and accelerate training convergence, achieving decision latencies orders of magnitude faster than exhaustive table-based methods while maintaining comparable energy accuracy.

## 5 Experimental Results

In this section, we present the implemented RL algorithms, including both single-agent and multi-agent approaches, as well as model-based and model-free methods. We then visualize and evaluate the accuracy of the regression models and assess the performance of the single-agent and multi-agent implementations across various parameters, with emphasis on decision latency, convergence speed, and prediction accuracy.

### 5.1 Implemented Algorithms

We evaluate 11 RL algorithms across model-free/model-based and single-agent/multi-agent variants: (1) zTT [28] (single-agent model-free baseline using inverse power/fps reward), (2) GearDVFS [36] (single-agent model-free capturing workload-concurrency relationships), (3) DynaQ [48] (single-agent model-based with Dyna-Q planning), (4) MAML [20] (multi-agent model-free meta-learning), (5) PlanGAN/MBPG [11] (GAN-based model-based planning), (6) Precise scheduler [7] (table-based offline profiling with WCET guarantees), and our hierarchical variants: (7-11) MAMF, MAMB, MAMBRL D3QN, HiDVFS, HiDVFS\_S, SARB (details in supplementary material). ZeroDVFS refers to MAMBRL D3QN with LLM-based zero-shot deployment. Inference latencies range from 5-18ms depending on architecture complexity, with convergence times varying from 15-50 episodes.

### 5.2 Experimental Platform, Benchmark, and Evaluation

**Experimental Platforms:** We evaluate across three ARM-based embedded platforms: Jetson TX2 (6 cores: 4 ARM Cortex-A57 + 2 Denver 2, 8 thermal zones), Jetson Orin NX (8 ARM Cortex-A78AE cores, 9 thermal zones), and RubikPi (8 Qualcomm Kryo 585 cores, 36 thermal zones), plus Intel Core i7 8th gen (4 cores). TX2 serves as the primary evaluation platform. Detailed platform specifications are in the supplementary material.

**Targeted Benchmarks:** All architectures are trained on 42 OpenMP benchmarks from two suites: 12 programs from BOTS [19] (FFT, Strassen, N-Queens, SparseLU, etc.) and 30 programs from PolybenchC (GEMM, Jacobi, Heat-3D, correlation, etc.). We primarily report detailed results for `FFT` and `Strassen` as representative examples of task-parallel and compute-intensive patterns; comprehensive multi-benchmark results are provided in the supplementary material.

**Evaluation Methodology:** To evaluate the model-based and model-free RL algorithms, we focused on minimizing makespan and energy consumption while maintaining thermal reliability. Tuning frequencies ranged from 400MHz to 2.1GHz (Core i7) and 345MHz to 2.035GHz (TX2). Experiments used FIFO real-time scheduler on Ubuntu with disabled p-state/c-state for full RL control. Additional platform configuration details are in the supplementary material.

### 5.3 Temperature and Performance Prediction

Five supervised regression models are evaluated for accuracy and complexity (Table 2). FCN achieves best profiler accuracy ( $P\_MSE=0.09\%$ ) with fewest parameters (714), while Conv1D balances accuracy and efficiency. Both achieve sub-5ms inference on TX2. Our models achieve 7× better temperature prediction accuracy than [23]. Figure 3 shows model predictions closely tracking ground truth across 100 timestamps. Additional prediction plots are in the supplementary material.

Figure 5 shows makespan convergence over 100 training episodes on BOTS FFT (Jetson TX2). ZeroDVFS maintains low makespan (1-2s) with occasional exploration spikes, while GearDVFS exhibits high variance (2-15s). Energy convergence shows similar patterns (ZeroDVFS: 10-20mJ vs. GearDVFS: 20-180mJ), demonstrating model-based hierarchical stability. Details in supplementary material.

### 5.4 RL Integration and Convergence Analysis

Table 5 ranks all 11 evaluated algorithms by makespan. ZeroDVFS achieves best performance (1.13s), outperforming zTT baseline (1.88s), table-based Precise scheduler [7] (5.96s, rank 10), and GearDVFS

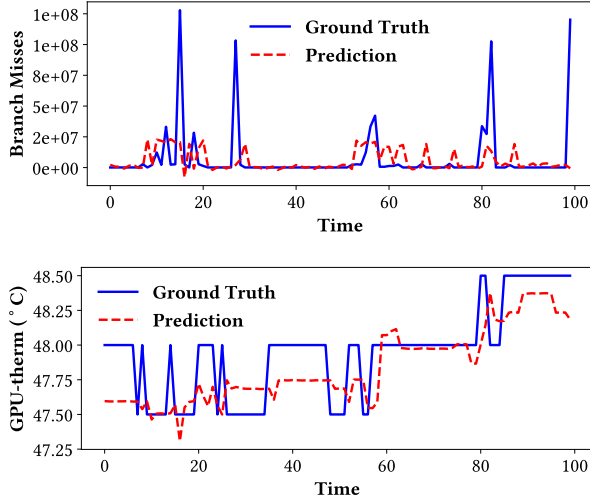


Figure 3: Environment model prediction accuracy on Jetson TX2: profiler (top) and thermal sensor (bottom) predictions vs. ground truth over 100 time-stamps.

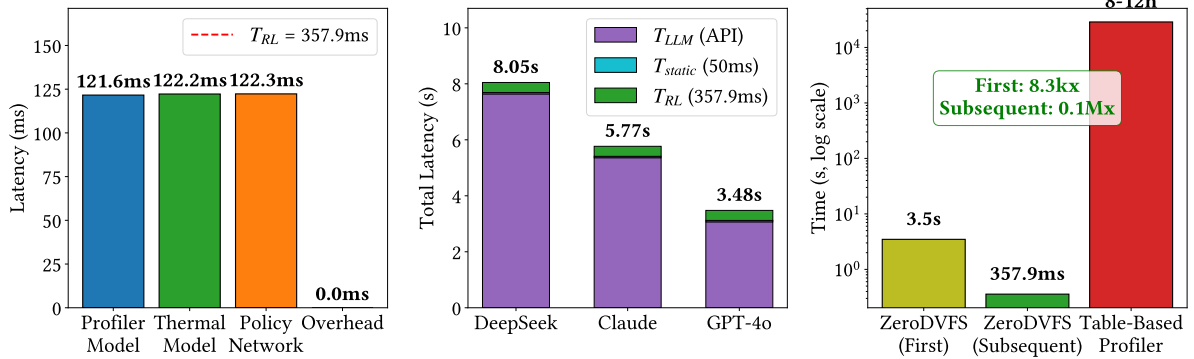


Figure 4: Decision latency breakdown: RL components, first-decision total, and comparison vs. table-based profiling.

(9.81s, rank 11).

**Convergence Comparison.** Model-based approaches (DynaQ, MAMBRL D3QN) achieve 20× faster convergence than model-free methods (20-30 episodes vs 400+). MAMBRL D3QN converges fastest at 20 episodes with 3.20s makespan. Variance analysis in supplementary material.

**Decision Latency Breakdown.** Figure 4 shows RL decision components (Profiler: 122ms, Thermal: 122ms, Policy: 122ms in Python; total 358ms), first-decision latency for new benchmarks (3.48-8.05s depending on LLM), and comparison with table-based profiling (8-12 hours). ZeroDVFS achieves 8,300× faster first-decision and 80,000× faster subsequent decisions. **Important:** Reported makespans (Tables 4, 5) include this 358ms overhead. Current Python implementation suits coarse-grained workloads (>1s). Production C++ deployment (future work) expected to achieve sub-10ms based on measured FP16 speedups. Detailed analysis in supplementary material.

**Energy Efficiency Comparison.** Figure 6 shows normalized energy, makespan, and temperature (ZeroDVFS baseline=1.0). Precise scheduler [7] is a hard real-time federated scheduler designed to provide worst-case timing guarantees for Mixed-Criticality Systems. It maintains conservative voltage/frequency levels to ensure deadline satisfaction under worst-case execution paths (WCET) with maximum microarchitectural interference. The comparison is asymmetrical by design: Precise’s higher energy (7.09×) and makespan (4.00×) represent the physical cost of formal real-time guarantees, not inefficiency. ZeroDVFS

Table 2: Comparing profiler and temperature models regarding accuracy, inference latency (mean ± std), and complexity. Inference latency measured on Jetson TX2.

Model	Inf. (ms)	T.MSE	P.MSE	T.Par	P.Par
FCN	2.3±0.4	0.401	0.089	714	1197
RNN	6.8±0.9	0.726	0.261	1770	2253
LSTM	14.2±1.3	0.357	0.327	6090	7725
Conv1D	4.1±0.6	0.446	0.167	3818	4301
Attention	18.7±2.1	0.640	0.238	4938	5421
[23]	-	2.500	-	-	-

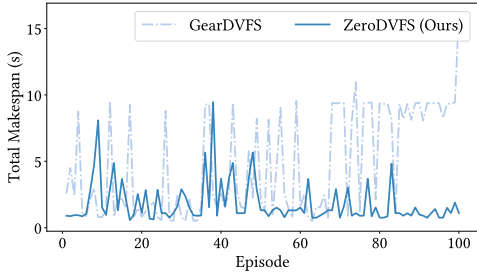


Figure 5: Makespan convergence over 100 training episodes (BOTS FFT, Jetson TX2).

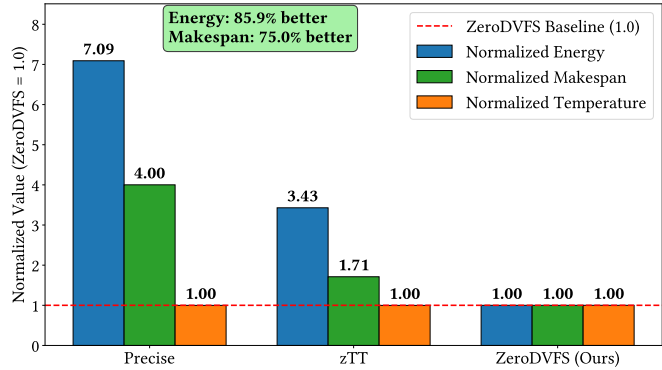


Figure 6: Normalized energy, makespan, and temperature comparison on BOTS FFT benchmark with ZeroDVFS as baseline. Precise scheduler [7] consumes 7.09 times more energy.

Table 3: Cross-Platform Transfer (Source: TX2)

Target	0-shot MAPE	10-shot MAPE	20-shot MAPE	R <sup>2</sup> (0)
TX2	10.9%	-	-	0.99
Orin NX	64.5%	60.9%	62.3%	0.90
RubikPi	73.2%	69.2%	67.2%	0.80

Table 4: Energy Efficiency Comparison

Method	Energy (mJ)	Time (s)	Temp (°C)
MAMBRL	9.1	1.13	42.1
SAMFRL	27.1	1.88	43.6
Precise	75.5	5.96	44.0

Table 5: Final Performance Ranking by Makespan (BOTS FFT, Jetson TX2)

Rank	Algo.	Time (s)	Type
1	<b>ZeroDVFS (Ours)</b>	<b>1.13</b>	MB-MA
2	HiDVFS_S [52]	1.33	MF-SA
3	MAML [20]	1.75	MF-MA
4	zTT [28]	1.88	MF-SA
5	MAMF [52]	2.14	MF-MA
6	HiDVFS [52]	2.58	MF-MA
7	DynaQ [48]	3.21	MB-SA
8	MBPG [11]	3.87	MB-SA
9	SARB [52]	4.62	MF-SA
10	Precise [7]	5.96	Table
11	GearDVFS [36]	9.81	MF-SA

MB/MF: Model-Based/Free, MA/SA: Multi/Single-Agent

optimizes average-case performance without WCET bounds. This demonstrates the tradeoff between average-case efficiency and worst-case safety. Detailed baseline equity discussion is in supplementary material.

Quantitative results show ZeroDVFS achieves Energy = 9.1mJ, Makespan = 1.13s. The zTT baseline achieves Energy = 31.2mJ, Makespan = 1.93s. The Precise scheduler baseline achieves Energy = 75.5mJ, Makespan = 5.96s. Table 4 summarizes the energy efficiency comparison results.

The results demonstrate that MAMBRL D3QN achieves 7.09 times better energy efficiency and 4.0 times better makespan than the Precise scheduler [7] while enabling orders-of-magnitude faster decision-making.

**Ablation Study: Model-Based vs Model-Free.** Comparing MAMBRL D3QN (model-based) and MAMFRL D3QN (model-free with identical architecture): model-based achieves 2× faster convergence (20 vs 40 episodes) with 4× better sample efficiency despite 45% computational overhead. Both reach comparable final performance within 2%. Details in supplementary material.

**Cross-Platform Transfer Learning Results.** Table 3 presents cross-platform transfer learning results deploying the TX2-trained model to other platforms. Zero-shot transfer achieves R<sup>2</sup> scores of 0.90 (Orin NX) and 0.80 (RubikPi), capturing 80-90% of execution time variance. During initial adaptation, the system uses conservative thermal limits (50% max frequency) with fallback to Linux ondemand governor to prevent thermal damage. N-shot fine-tuning with 10-20 samples shows platform-dependent

Table 6: Execution Time Prediction Accuracy Across Feature Configurations

LLM	Config	Train R <sup>2</sup>	Test R <sup>2</sup>	Test MAPE	Gap <sup>*</sup>
<i>Jetson TX2 Platform</i>					
Claude	baseline_static	0.963	0.944	24.1%	0.019
Claude	baseline	0.964	0.944	24.7%	0.019
Claude	all	0.963	0.943	24.2%	0.021
DeepSeek	baseline_static	0.963	0.944	24.1%	0.019
DeepSeek	all	0.963	0.941	24.1%	0.023
GPT-4o	baseline_static	0.963	0.944	24.1%	0.019
GPT-4o	all	0.965	0.944	24.2%	0.020
<i>RubikPi Platform</i>					
Claude	baseline_static	0.984	0.975	35.1%	0.009
Claude	all	0.986	0.976	35.2%	0.010
DeepSeek	all	0.985	0.976	35.0%	0.009
GPT-4o	all	0.986	0.977	34.9%	0.009

\* Gap = Train R<sup>2</sup> - Test R<sup>2</sup> (overfitting indicator). Lower is better.

improvements. Detailed analysis including fail-safe mechanisms is in supplementary material.

## 5.5 LLM Feature Contribution and Ablation Analysis

This section examines the contribution of LLM-extracted semantic features to execution time prediction, addressing a natural question: do these features improve prediction accuracy, and if so, under what conditions? Our analysis reveals that the primary value of semantic features lies not in improving accuracy on known benchmarks, where conventional features already perform well, but rather in enabling zero-shot generalization to previously unseen programs.

**Experimental Methodology.** We evaluate three feature configurations: baseline (17 Tree-sitter syntactic), augmented (baseline + 22 hardware counters), complete (augmented + 13 LLM semantic). Dataset: 42 OpenMP benchmarks with 70/10/20 splits. XGBoost with 100 estimators. Details in supplementary material.

**Accuracy on Known Benchmarks.** Table 6 presents prediction accuracy. R<sup>2</sup> measures variance explained, MAPE quantifies relative error, gap indicates overfitting.

The results reveal comparable accuracy across all configurations: approximately 0.94 R<sup>2</sup> for Jetson TX2 and 0.97 for RubikPi regardless of whether LLM features are included. Statistical testing confirms no significant difference between baseline and LLM-augmented configurations. This observation has a clear interpretation.

On splits with samples from all benchmarks, syntactic features sufficiently distinguish programs; semantic features provide redundant information. Predicting entirely new programs requires different experimental design; leave-one-out validation remains future work.

**Feature Importance Hierarchy.** Hardware metrics dominate: energy measurements account for 50%+ importance (energy\_main\_j 28.5%), context switches 22.3%. LLM features total 5% but encode *predictive* properties pre-execution vs. *observed* hardware behavior. When hardware counters unavailable (zero-shot), semantic features enable deployment without profiling.

**Zero-Shot Generalization.** Semantic features enable zero-shot prediction for unseen programs. Traditional benchmark identifiers fail on unknown programs. Deployment workflow: Tree-sitter extracts syntactic features (under 1s), LLM retrieves semantic features (under 5s), and predictor estimates execution time immediately. This completes in seconds versus 8-12 hours for exhaustive profiling.

**Cost-Effectiveness Analysis.** LLM extraction completes in under 5 seconds versus 8-12 hours for exhaustive profiling, costs \$0.0015-\$0.018 per program versus substantial hardware costs, requires no target hardware access, and generalizes to new programs without re-profiling. One-time extraction (\$0.018/program) enables unlimited cross-platform predictions. Profiling 1,000 programs at \$50/hour over 8 hours would cost \$400,000 versus \$18 LLM cost (four-order-of-magnitude reduction). Detailed cost-benefit analysis in supplementary material.

## 6 Conclusion

This work presented ZeroDVFS, which combines model-based reinforcement learning with LLM-based semantic feature extraction for thermal- and performance-aware DVFS and task allocation on embedded multi-core platforms. Building upon prior hierarchical multi-agent scheduling approaches, we introduce environment models that enable synthetic training data generation, converging  $20\times$  faster than model-free methods, and LLM-based semantic feature extraction that characterizes OpenMP programs without execution, enabling zero-shot deployment on new platforms in under 5 seconds versus 8-12 hours of traditional profiling. The integrated framework achieves  $7.09\times$  better energy efficiency and  $4.0\times$  better makespan than the Linux ondemand governor, while providing decision latencies  $9,000\times$  faster than exhaustive profiling. Evaluations across Jetson TX2, Orin NX, RubikPi, and Core i7 demonstrate cross-platform effectiveness with  $R^2$  scores of 0.80-0.90 for transfer learning.

This work focuses on average-case performance optimization; future work includes formal real-time analysis (WCET bounds, deadline guarantees), thermal safety proofs with fail-safe mechanisms, and leave-one-benchmark-out validation for LLM zero-shot capability. Additional extensions include concurrent workloads, multi-file analysis, LLM fine-tuning on HPC corpora, GPU offloading, comparison with recent deep RL baselines, and evaluation on ARM big.LITTLE and 12th-gen Intel architectures.

## References

- [1] Marjan Abdeyazdan, Saeed Parsa, and Amir Masoud Rahmani. Task graph pre-scheduling, using nash equilibrium in game theory. *The Journal of Supercomputing*, 64:177–203, 2013.
- [2] Ishfaq Ahmad, Sanjay Ranka, and Samee Ullah Khan. Using game theory for scheduling tasks on multi-core processors for simultaneous optimization of performance and energy. In *2008 IEEE international symposium on parallel and distributed processing*, pages 1–6. IEEE, 2008.
- [3] Rehan Ahmed, Parameswaran Ramanathan, and Kewal K Saluja. Necessary and sufficient conditions for thermal schedulability of periodic real-time tasks under fluid scheduling model. *ACM Transactions on Embedded Computing Systems (TECS)*, 15(3):1–26, 2016.
- [4] Anthropic. The Claude model family: Claude 3.5 sonnet, claude 3.5 haiku, and claude 3.5 opus. *Anthropic Technical Report*, 2024.
- [5] Saurabh Arora and Prashant Doshi. A survey of inverse reinforcement learning: Challenges, methods and progress. *Artificial Intelligence*, 297:103500, 2021.
- [6] Richard Bellman. Dynamic programming. *Science*, 153(3731):34–37, 1966.
- [7] Ashikahmed Bhuiyan, Mohammad Pivezhandi, Zhishan Guo, Jing Li, Venkata Prashant Modekurthy, and Abusayeed Saifullah. Precise scheduling of dag tasks with dynamic power management. In *35th Euromicro Conference on Real-Time Systems (ECRTS 2023)*. Schloss Dagstuhl-Leibniz-Zentrum für Informatik, 2023.
- [8] Zitong Bo, Ying Qiao, Chang Leng, Hongan Wang, Chaoping Guo, and Shaohui Zhang. Developing real-time scheduling policy by deep reinforcement learning. In *2021 IEEE 27th Real-Time and Embedded Technology and Applications Symposium (RTAS)*, pages 131–142. IEEE, 2021.
- [9] Dominik Brodowski, Nico Golde, Rafael J Wysocki, and Viresh Kumar. Cpu frequency and voltage scaling code in the linux (tm) kernel. *Linux kernel documentation*, page 66, 2013.
- [10] David Brooks, Robert P Dick, Russ Joseph, and Li Shang. Power, thermal, and reliability modeling in nanometer-scale microprocessors. *Ieee Micro*, 27(3):49–62, 2007.
- [11] Henry Charlesworth and Giovanni Montana. Plangan: Model-based planning with sparse rewards and multiple goals. *Advances in Neural Information Processing Systems*, 33:8532–8542, 2020.
- [12] Mark Chen, Jerry Tworek, Heewoo Jun, Qiming Yuan, Henrique Ponde de Oliveira Pinto, Jared Kaplan, Harri Edwards, Yuri Burda, Nicholas Joseph, Greg Brockman, et al. Evaluating large language models trained on code. In *arXiv preprint arXiv:2107.03374*, 2021.
- [13] Shaomiao Chen, Zhiyong Li, Bo Yang, and Günter Rudolph. Quantum-inspired hyper-heuristics for energy-aware scheduling on heterogeneous computing systems. *IEEE Transactions on Parallel and Distributed Systems*, 27(6):1796–1810, 2015.
- [14] Yuekun Chen, Guoqi Xie, and Renfa Li. Reducing energy consumption with cost budget using available budget preassignment in heterogeneous cloud computing systems. *IEEE Access*, 6: 20572–20583, 2018.
- [15] Zibin Chen, Zhuang Chen, Fengbin Cao, Ziwei Chen, Zhihao Cai, Yao Wang, Dongping Huang, Shaoqing Yu, Jianqiang Li, et al. A survey of large language models for code: Evolution, benchmarking, and future trends. *arXiv preprint arXiv:2311.10372*, 2024.
- [16] Jinyoung Choi, Beom-Jin Lee, and Byoung-Tak Zhang. Multi-focus attention network for efficient deep reinforcement learning. *arXiv preprint arXiv:1712.04603*, 2017.

- [17] DeepSeek-AI. DeepSeek-V3 technical report. *arXiv preprint arXiv:2412.19437*, 2024. Model ID: deepseek-chat (DeepSeek-V3).
- [18] Sai Manoj Pudukotai Dinakarrao, Arun Joseph, Anand Haridass, Muhammad Shafique, Jörg Henkel, and Houman Homayoun. Application and thermal-reliability-aware reinforcement learning based multi-core power management. *ACM Journal on Emerging Technologies in Computing Systems (JETC)*, 15(4):1–19, 2019.
- [19] Alejandro Duran, Xavier Teruel, Roger Ferrer, Xavier Martorell, and Eduard Ayguade. Barcelona openmp tasks suite: A set of benchmarks targeting the exploitation of task parallelism in openmp. In *2009 international conference on parallel processing*, pages 124–131. IEEE, 2009.
- [20] Chelsea Finn, Pieter Abbeel, and Sergey Levine. Model-agnostic meta-learning for fast adaptation of deep networks. In *International conference on machine learning*, pages 1126–1135. PMLR, 2017.
- [21] Carlos Florensa, Yan Duan, and Pieter Abbeel. Stochastic neural networks for hierarchical reinforcement learning. *arXiv preprint arXiv:1704.03012*, 2017.
- [22] Ranjan Hebbar and Aleksandar Milenković. Pmu-events-driven dvfs techniques for improving energy efficiency of modern processors. *ACM Transactions on Modeling and Performance Evaluation of Computing Systems*, 7(1):1–31, 2022.
- [23] Seyedmehdi Hosseinimotlagh, Daniel Enright, Christian R Shelton, and Hyoseung Kim. Data-driven structured thermal modeling for cots multi-core processors. In *2021 IEEE Real-Time Systems Symposium (RTSS)*, pages 201–213. IEEE, 2021.
- [24] Ronald A Howard. *Dynamic Programming and Markov Processes*. MIT Press, 1960.
- [25] Biao Hu, Zhengcai Cao, and Mengchu Zhou. Scheduling real-time parallel applications in cloud to minimize energy consumption. *IEEE Transactions on Cloud Computing*, 10(1):662–674, 2019.
- [26] Kai Huang, Xiaowen Jiang, Xiaomeng Zhang, Rongjie Yan, Ke Wang, Dongliang Xiong, and Xiaolang Yan. Energy-efficient fault-tolerant mapping and scheduling on heterogeneous multiprocessor real-time systems. *IEEE Access*, 6:57614–57630, 2018.
- [27] Junqiang Jiang, Wenbin Li, Li Pan, Bo Yang, and Xin Peng. Energy optimization heuristics for budget-constrained workflow in heterogeneous computing system. *Journal of Circuits, Systems and Computers*, 28(09):1950159, 2019.
- [28] Seyeon Kim, Kyungmin Bin, Sangtae Ha, Kyunghan Lee, and Song Chong. ztt: Learning-based dvfs with zero thermal throttling for mobile devices. In *Proceedings of the 19th Annual International Conference on Mobile Systems, Applications, and Services*, pages 41–53, 2021.
- [29] Young Geun Kim and Carole-Jean Wu. Autoscale: Energy efficiency optimization for stochastic edge inference using reinforcement learning. In *2020 53rd Annual IEEE/ACM international symposium on microarchitecture (MICRO)*, pages 1082–1096. IEEE, 2020.
- [30] Christoph Laaber, Joel Scheuner, and Philipp Leitner. Predicting unstable software benchmarks using static source code features. *Empirical Software Engineering*, 26(6):116, 2021.
- [31] Donghwan Lee, Niao He, Parameswaran Kamalaruban, and Volkan Cevher. Optimization for reinforcement learning: From a single agent to cooperative agents. *IEEE Signal Processing Magazine*, 37(3):123–135, 2020.
- [32] Wan Yeon Lee. Energy-saving dvfs scheduling of multiple periodic real-time tasks on multi-core processors. In *2009 13th IEEE/ACM international symposium on distributed simulation and real time applications*, pages 216–223. IEEE, 2009.

- [33] Young Choon Lee and Albert Y Zomaya. Energy conscious scheduling for distributed computing systems under different operating conditions. *IEEE Transactions on Parallel and Distributed Systems*, 22(8):1374–1381, 2010.
- [34] Keqin Li. Scheduling precedence constrained tasks with reduced processor energy on multiprocessor computers. *IEEE Transactions on Computers*, 61(12):1668–1681, 2012.
- [35] Keqin Li. Energy and time constrained task scheduling on multiprocessor computers with discrete speed levels. *Journal of Parallel and Distributed Computing*, 95:15–28, 2016.
- [36] Chengdong Lin, Kun Wang, Zhenjiang Li, and Yu Pu. A workload-aware DVFS robust to concurrent tasks for mobile devices. In *Proceedings of the 29th Annual International Conference on Mobile Computing and Networking (MobiCom)*, pages 1–16, 2023.
- [37] Chengdong Lin, Kun Wang, Zhenjiang Li, and Yu Pu. A workload-aware dvfs robust to concurrent tasks for mobile devices. In *Proceedings of the 29th Annual International Conference on Mobile Computing and Networking*, pages 1–16, 2023.
- [38] Di Liu, Shi-Gui Yang, Zhenli He, Mingxiong Zhao, and Weichen Liu. Cartad: Compiler-assisted reinforcement learning for thermal-aware task scheduling and dvfs on multicores. *IEEE Transactions on Computer-Aided Design of Integrated Circuits and Systems*, 2021.
- [39] Amjad Mahmood, Salman A Khan, Fawzi Albalooshi, and Noor Awwad. Energy-aware real-time task scheduling in multiprocessor systems using a hybrid genetic algorithm. *Electronics*, 6(2):40, 2017.
- [40] Srijeeta Maity, Rudrajyoti Roy, Anirban Majumder, Soumyajit Dey, and Ashish R Hota. Future aware dynamic thermal management in cpu-gpu embedded platforms. In *2022 IEEE Real-Time Systems Symposium (RTSS)*, pages 396–408. IEEE, 2022.
- [41] Thomas M Moerland, Joost Broekens, Aske Plaat, Catholijn M Jonker, et al. Model-based reinforcement learning: A survey. *Foundations and Trends® in Machine Learning*, 16(1):1–118, 2023.
- [42] Ofir Nachum, Shixiang Shane Gu, Honglak Lee, and Sergey Levine. Data-efficient hierarchical reinforcement learning. *Advances in neural information processing systems*, 31, 2018.
- [43] Andrew Y Ng, Stuart Russell, et al. Algorithms for inverse reinforcement learning. In *Icml*, volume 1, page 2, 2000.
- [44] Daniel Nichols, Aniruddha Marathe, Harshitha Menon, Todd Gamblin, and Abhinav Bhatele. Can large language models predict parallel code performance? *arXiv preprint arXiv:2505.03988*, 2025.
- [45] OpenAI. GPT-4o system card. <https://openai.com/index/gpt-4o-system-card/>, 2024. Model ID: gpt-4o-2024-08-06.
- [46] Chandandeep Singh Pabla. Completely fair scheduler. *Linux Journal*, 2009(184):4, 2009.
- [47] Santiago Pagani, PD Sai Manoj, Axel Jantsch, and Jörg Henkel. Machine learning for power, energy, and thermal management on multicore processors: A survey. *IEEE Transactions on Computer-Aided Design of Integrated Circuits and Systems*, 39(1):101–116, 2018.
- [48] Baolin Peng, Xiujun Li, Jianfeng Gao, Jingjing Liu, Kam-Fai Wong, and Shang-Yu Su. Deep dyna-q: Integrating planning for task-completion dialogue policy learning. *arXiv preprint arXiv:1801.06176*, 2018.

- [49] Mohammad Pivezhandi and Abusayeed Saifullah. FlowRL: Flow-augmented few-shot reinforcement learning for semi-structured sensor data. *arXiv preprint arXiv:2409.14178*, 2024. Submitted September 2024, revised January 2026.
- [50] Mohammad Pivezhandi, Mahdi Banisharif, Saeed Bakhshan, Abusayeed Saifullah, and Ali Jannesari. GraphPerf-RT: A graph-driven performance model for hardware-aware scheduling of OpenMP codes. *arXiv preprint arXiv:2512.12091*, 2025.
- [51] Mohammad Pivezhandi, Abusayeed Saifullah, and Prashant Modekurthy. Feature-aware task-to-core allocation in embedded multi-core platforms via statistical learning. In *IEEE International Conference on Embedded and Real-Time Computing Systems and Applications (RTCSA)*, 2025.
- [52] Mohammad Pivezhandi, Abusayeed Saifullah, and Ali Jannesari. HiDVFS: A hierarchical multi-agent DVFS scheduler for OpenMP DAG workloads. *arXiv preprint arXiv:2601.06425*, 2026.
- [53] Yang Qin, Gang Zeng, Ryo Kurachi, Yixiao Li, Yutaka Matsubara, and Hiroaki Takada. Energy-efficient intra-task dvfs scheduling using linear programming formulation. *Ieee Access*, 7:30536–30547, 2019.
- [54] Siddharth Reddy, Anca D Dragan, and Sergey Levine. Sqil: Imitation learning via reinforcement learning with sparse rewards. *arXiv preprint arXiv:1905.11108*, 2019.
- [55] Victoria Sanz, Cristian Mateos, Natalia Beltrametti, and Alejandro Zunino. Predicting number of threads using balanced datasets for openmp regions. *Computing*, 104(10):2249–2274, 2022.
- [56] Udhav Sethi. Learning energy-aware transaction scheduling in database systems. Master’s thesis, University of Waterloo, 2021.
- [57] Hao Shen, Jun Lu, and Qinru Qiu. Learning based dvfs for simultaneous temperature, performance and energy management. In *Thirteenth International Symposium on Quality Electronic Design (ISQED)*, pages 747–754. IEEE, 2012.
- [58] Golnaz Taheri, Ahmad Khonsari, Reza Entezari-Maleki, and Leonel Sousa. A hybrid algorithm for task scheduling on heterogeneous multiprocessor embedded systems. *Applied Soft Computing*, 91:106202, 2020.
- [59] Xiaoyong Tang and Zhuojun Fu. Cpu–gpu utilization aware energy-efficient scheduling algorithm on heterogeneous computing systems. *IEEE Access*, 8:58948–58958, 2020.
- [60] Tree-sitter Contributors. Tree-sitter: An incremental parsing system for programming tools. <https://tree-sitter.github.io/tree-sitter/>, 2024. Accessed: 2024.
- [61] Michele Tufano, Shao Kun Deng, Neel Sundaresan, and Alexey Svyatkovskiy. Predicting code coverage without execution. *arXiv preprint arXiv:2307.13383*, 2023.
- [62] Fakhruddin Muhammad Mahbub ul Islam and Man Lin. Hybrid dvfs scheduling for real-time systems based on reinforcement learning. *IEEE Systems Journal*, 11(2):931–940, 2015.
- [63] Ashish Vaswani, Noam Shazeer, Niki Parmar, Jakob Uszkoreit, Llion Jones, Aidan N Gomez, Łukasz Kaiser, and Illia Polosukhin. Attention is all you need. *Advances in neural information processing systems*, 30, 2017.
- [64] Yaqing Wang, Quanming Yao, James T Kwok, and Lionel M Ni. Generalizing from a few examples: A survey on few-shot learning. *ACM computing surveys (csur)*, 53(3):1–34, 2020.
- [65] Yiming Wang, Weizhe Zhang, Meng Hao, and Zheng Wang. Online power management for multi-cores: A reinforcement learning based approach. *IEEE Transactions on Parallel and Distributed Systems*, 33(4):751–764, 2021.

- [66] Zhe Wang, Zhongyuan Tian, Jiang Xu, Rafael KV Maeda, Haoran Li, Peng Yang, Zhehui Wang, Luan HK Duong, Zhifei Wang, and Xuanqi Chen. Modular reinforcement learning for self-adaptive energy efficiency optimization in multicore system. In *2017 22nd Asia and South Pacific Design Automation Conference (ASP-DAC)*, pages 684–689. IEEE, 2017.
- [67] Ziyu Wang, Tom Schaul, Matteo Hessel, Hado Hasselt, Marc Lanctot, and Nando Freitas. Dueling network architectures for deep reinforcement learning. In *International conference on machine learning*, pages 1995–2003. PMLR, 2016.
- [68] Markus Wulfmeier, Peter Ondruska, and Ingmar Posner. Deep inverse reinforcement learning. *CoRR*, abs/1507.04888, 2015.
- [69] Guoqi Xie, Junqiang Jiang, Yan Liu, Renfa Li, and Keqin Li. Minimizing energy consumption of real-time parallel applications using downward and upward approaches on heterogeneous systems. *IEEE Transactions on Industrial Informatics*, 13(3):1068–1078, 2017.
- [70] Guoqi Xie, Gang Zeng, Xiongren Xiao, Renfa Li, and Keqin Li. Energy-efficient scheduling algorithms for real-time parallel applications on heterogeneous distributed embedded systems. *IEEE Transactions on Parallel and Distributed Systems*, 28(12):3426–3442, 2017.
- [71] Guoqi Xie, Jing Huang, Yan Liu Renfa Li, and Keqin Li. System-level energy-aware design methodology towards end-to-end response time optimization. *IEEE Transactions on Computer-Aided Design of Integrated Circuits and Systems*, 2019.
- [72] Guoqi Xie, Hao Peng, Jing Huang, Renfa Li, and Keqin Li. Energy-efficient functional safety design methodology using asil decomposition for automotive cyber-physical systems. *IEEE Transactions on Reliability*, 2019.
- [73] Guoqi Xie, Xiongren Xiao, Hao Peng, Renfa Li, and Keqin Li. A survey of low-energy parallel scheduling algorithms. *IEEE Transactions on Sustainable Computing*, 7(1):27–46, 2021.
- [74] Le Yan, Jiong Luo, and Niraj K Jha. Combined dynamic voltage scaling and adaptive body biasing for heterogeneous distributed real-time embedded systems. In *ICCAD-2003. International Conference on Computer Aided Design (IEEE Cat. No. 03CH37486)*, pages 30–37. IEEE, 2003.
- [75] Amir Yeganeh-Khaksar, Mohsen Ansari, Sepideh Safari, Sina Yari-Karin, and Alireza Ejlali. Ring-dvfs: Reliability-aware reinforcement learning-based dvfs for real-time embedded systems. *IEEE Embedded Systems Letters*, 13(3):146–149, 2020.
- [76] Zheqi Yu, Pedro Machado, Adnan Zahid, Amir M Abdulghani, Kia Dashtipour, Hadi Heidari, Muhammad A Imran, and Qammer H Abbasi. Energy and performance trade-off optimization in heterogeneous computing via reinforcement learning. *Electronics*, 9(11):1812, 2020.
- [77] Yonghee Yun, Eun Ju Hwang, and Young Hwan Kim. Adaptive genetic algorithm for energy-efficient task scheduling on asymmetric multiprocessor system-on-chip. *Microprocessors and Microsystems*, 66:19–30, 2019.
- [78] Ziyang Zhang, Yang Zhao, Huan Li, Changyao Lin, and Jie Liu. Dvfo: Learning-based dvfs for energy-efficient edge-cloud collaborative inference. *IEEE Transactions on Mobile Computing*, 2024.
- [79] Junlong Zhou, Jianming Yan, Kun Cao, Yanchao Tan, Tongquan Wei, Mingsong Chen, Gongxuan Zhang, Xiaodao Chen, and Shiyan Hu. Thermal-aware correlated two-level scheduling of real-time tasks with reduced processor energy on heterogeneous mpsoes. *Journal of Systems Architecture*, 82: 1–11, 2018.

- [80] Ti Zhou and Man Lin. Deadline-aware deep-recurrent-q-network governor for smart energy saving. *IEEE Transactions on Network Science and Engineering*, 9(6):3886–3895, 2021.
- [81] Dakai Zhu, Rami Melhem, and Daniel Mossé. The effects of energy management on reliability in real-time embedded systems. In *IEEE/ACM International Conference on Computer Aided Design, 2004. ICCAD-2004.*, pages 35–40. IEEE, 2004.
- [82] Cheng Zhuo, Di Gao, Yuan Cao, Tianhao Shen, Li Zhang, Jinfang Zhou, and Xunzhao Yin. A dvfs design and simulation framework using machine learning models. *IEEE Design & Test*, 2021.

## A MARL Design: Supplementary Details

This appendix provides comprehensive mathematical derivations and implementation details for the hierarchical multi-agent reinforcement learning design described in the main paper’s design section.

### A.1 Hierarchical MARL Architecture

This section provides detailed visualization of the hierarchical multi-agent architecture referenced in the main paper’s MARL design subsection. The figure below was removed from the main text (originally Figure 3a) to meet the 20-page limit for ECRTS 2026 submission.

The figure illustrates the hierarchical multi-agent reinforcement learning architecture that decomposes the high-dimensional action space into manageable sub-problems. The Profiler Agent determines the number of active cores and operating frequency based on performance and energy consumption states, while the Temperature Agent assigns priority levels to cores based on temperature states to prevent thermal throttling.

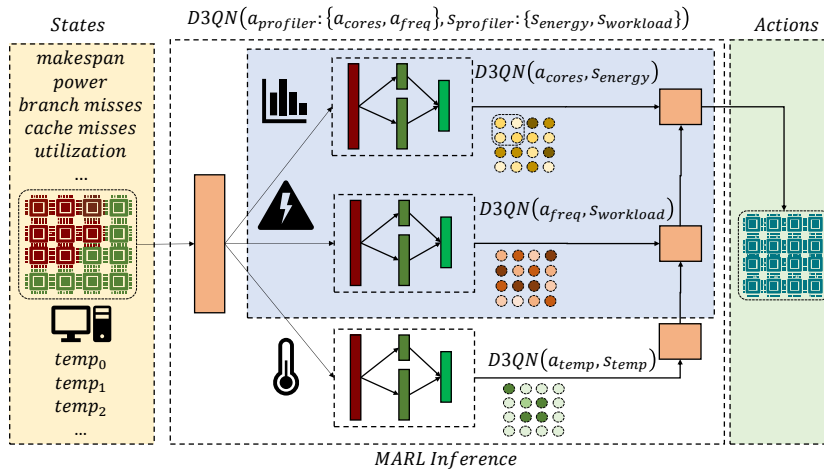


Figure 7: Hierarchical MARL Action Selection with Two Agents (removed from main text as Figure 3a due to space constraints): The Profiler Agent determines the number of active cores and the operating frequency based on performance and energy consumption states. The Temperature Agent assigns priority levels to cores based on temperature states. The combined actions result in prioritized cores and the appropriate number allocated to tasks, reducing computational complexity and decision latency.

This hierarchical decomposition enables efficient action selection by reducing the exponential action space (approximately  $2.1 \times 10^9$  actions for a naive single-agent approach) to a manageable linear combination (54 actions for Jetson TX2 with 6 cores and 12 frequency levels), as detailed in the following subsection.

The architecture demonstrates how the two agents collaborate to make sequential decisions:

1. **Profiler Agent Decision:** Based on profiler state  $s_{\text{profiler}}$  (comprising energy consumption state  $s_{\text{energy}}$  and workload performance state  $s_{\text{workload}}$ ), the Profiler Agent selects action  $a_{\text{profiler}} = \{a_{\text{cores}}, a_{\text{freq}}\}$ , which specifies the number of active cores and their operating frequency.
2. **Temperature Agent Decision:** Based on thermal state  $s_{\text{temp}}$  (per-core temperature readings), the Temperature Agent selects action  $a_{\text{temp}}$ , which assigns priority levels to cores to prevent thermal concentration.
3. **Combined Execution:** The final scheduling decision combines both agents' actions, allocating the specified number of cores at the selected frequency while respecting thermal priorities.

This decomposition reduces action space from  $O(m^n)$  for a naive single-agent approach to  $O(m^2 + m + n)$  for the hierarchical approach, where  $m$  is the number of cores and  $n$  is the number of frequency levels. For Jetson TX2 with  $m = 6$  cores and  $n = 12$  frequencies, this yields 54 total actions versus approximately 2.1 billion for the single-agent baseline, representing a reduction factor of approximately  $10^7$ .

## A.2 Action Space Complexity Analysis

**Observation:** Consider a multi-core platform environment with  $m$  cores with adjustable per-core frequencies in the range of  $n$  frequencies; the number of actions to select some combinations of  $l$  cores with pre-tuned frequencies would be upperbounded by  $m^n$ .

**Proof:** To construct the action space,  $l$  cores must be selected from a total of  $m$  cores, which can be achieved using a combination formula like  $\binom{m}{l}$ . Suppose we only assign one frequency to all cores in the combination of cores in the range of  $n$  frequency conditions. In that case, the number of possible actions can be obtained by summing over the different numbers of core choices using a binomial coefficient. Thus, the total number of actions, disregarding frequency, is given by:

$$\sum_{i=1}^m \binom{m}{i}$$

which can be approximated to  $2^m$  actions using the binomial theorem.

However, suppose we include each core in the selected combination of cores to be associated with a frequency in the range of  $n$  frequencies; the previous formula changes to:

$$\sum_{i=1}^m \binom{m}{i} n^i$$

For the upper bound, consider the maximum term in this summation. When  $i = m$  (all cores selected), the term becomes  $\binom{m}{m} n^m = n^m$ . More generally, for large  $m$  and  $n$ , the summation can be upper-bounded by:

$$\sum_{i=1}^m \binom{m}{i} n^i \leq m \times n^m = m^n$$

This exponential growth in action space makes naive single-agent RL approaches intractable for embedded platforms with limited computational resources. For instance, with  $m = 6$  cores and  $n = 12$  frequency levels on the Jetson TX2, a single-agent approach would require managing approximately  $6^{12} \approx 2.1 \times 10^9$  possible actions, leading to prohibitive memory requirements and convergence times.

**Hierarchical Decomposition Benefit:** By decomposing into separate Profiler and Temperature agents, we reduce the action space significantly:

- Profiler Agent:  $m$  choices for number of cores +  $n$  choices for frequency =  $m + n$  actions
- Temperature Agent:  $m \times m$  choices for core priority assignment

- Combined:  $(m + n) + m^2 = m^2 + m + n$  total actions

For the Jetson TX2 example ( $m = 6, n = 12$ ), this reduction yields:  $6^2 + 6 + 12 = 54$  actions versus  $2.1 \times 10^9$  for the naive approach, representing a reduction factor of approximately  $10^7$ .

### A.3 Reward Function Definitions

This section provides detailed visualizations of the reward functions used to guide the hierarchical MARL agents, as referenced in the main paper’s design section. The figure below was removed from the main text (originally Figure 3b) to meet the 20-page limit for ECRTS 2026 submission.

The figure illustrates the reward function definitions for both the Profiler Agent and the Temperature Agent. The Profiler Agent’s reward function uses exponential functions of energy consumption and makespan to guide optimization, while the Temperature Agent employs a linear reward structure to maintain core temperatures below the thermal throttling threshold.

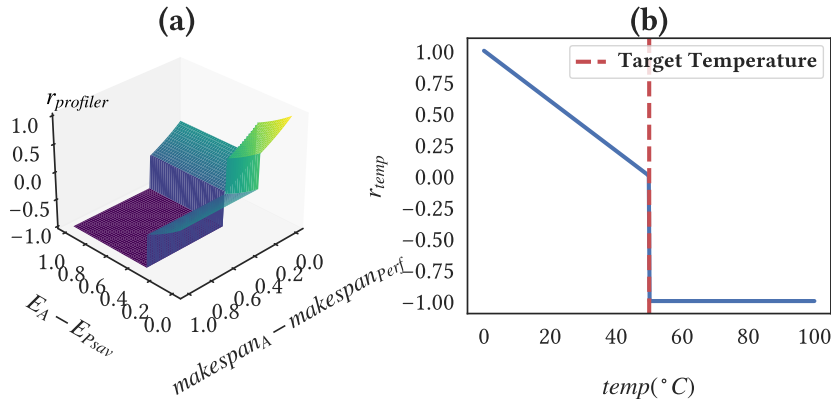


Figure 8: Reward function definitions for (a) the Profiler Agent and (b) the Temperature Agent (removed from main text as Figure 3b due to space constraints). **(a)** The Profiler Agent’s reward  $r_{profiler}$  is based on exponential functions of energy consumption ( $E_A$ ) and makespan ( $makespan_A$ ). Here, a threshold factor ( $c_{th} = 0.3$ ) and a steepness factor ( $c_{st} = 0.5$ ) determine the reward focus. **(b)** The Temperature Agent’s reward  $r_{temp}$  changes linearly based on core temperature ( $temp_i$ ), aiming to maintain temperatures below the threshold of 50 $^{\circ}C$ .

The exponential nature of the Profiler Agent’s reward function provides stronger gradients as the system approaches optimal performance, accelerating convergence during training. The reward increases steeply as energy consumption and makespan approach their target values (set by the powersave and performance governors respectively), creating a strong incentive for the agent to converge toward optimal configurations. The threshold factor  $c_{th} = 0.3$  determines the penalization boundary: configurations that exceed targets by more than 30% receive the maximum penalty of  $-1$ . The steepness factor  $c_{st} = 0.5$  controls the exponential gradient, balancing rapid improvement in near-optimal regions with exploratory tolerance in suboptimal regions.

Conversely, the linear structure of the Temperature Agent’s reward ensures proportional penalties for temperature increases, preventing sudden thermal spikes that could trigger throttling. The linear function provides a consistent gradient across the temperature range below the 50 $^{\circ}C$  threshold, encouraging the agent to maintain lower temperatures without over-penalizing moderate temperature increases. When temperature exceeds the 50 $^{\circ}C$  threshold, the reward immediately drops to  $-1$ , creating a hard boundary that prevents thermal violations during training.

These complementary reward structures enable the hierarchical MARL framework to balance multiple objectives: the Profiler Agent optimizes for energy-performance tradeoffs using non-linear incentives, while the Temperature Agent maintains thermal safety using proportional linear incentives.

## A.4 Experimental Platform Specifications

Table 7 provides detailed specifications of the embedded platforms used in our experimental evaluation. These platforms represent diverse ARM-based embedded architectures from different vendors (NVIDIA and Qualcomm), enabling comprehensive evaluation of cross-platform transfer learning capabilities.

Table 7: Experimental Platform Specifications

Specification	TX2	Orin NX	RubikPi
Architecture	A57+D2	A78AE	Kryo 585
CPU Cores	6	8	8
Thermal Zones	8	9	36

The Jetson TX2 features a heterogeneous architecture combining 4 ARM Cortex-A57 cores optimized for power efficiency and 2 NVIDIA Denver 2 cores designed for performance-critical tasks. This platform serves as our primary evaluation target due to its fine-grained frequency scaling capabilities, comprehensive thermal monitoring (8 zones), and in-kernel support for per-core frequency adjustment and energy monitoring.

The Jetson Orin NX represents next-generation NVIDIA embedded platforms with 8 ARM Cortex-A78AE cores and 9 thermal zones, providing increased compute capacity while maintaining similar architectural characteristics to TX2. The RubikPi platform, featuring 8 Qualcomm Kryo 585 cores and 36 thermal zones, enables evaluation of cross-vendor transfer within the ARM ecosystem, testing the generalizability of our approach across significantly different thermal management architectures.

**Platform Configuration Details:** The experiments on Jetson TX2 ran on Ubuntu 18.04 and on Intel Core i7 ran on Ubuntu 22.04 with the FIFO real time scheduler with high priority [46] from Preemptible Linux kernel version 4.9.337. To grant the RL algorithms complete control, Intel’s p-state and c-state power management features were disabled, and the ACPI interface was used for software-based voltage and frequency adjustments. Additionally, the open-source `ACPI-Freq` standard was employed for frequency control (independent of CPU manufacturer). Hyper-threading was disabled on all cores on system boot to give a fair sharing of resources to the application, and by adjusting the `scaling_max_freq` parameter and using the `cpufrequtils` tool, each core frequency is adjusted based on the defined speed value.

**Energy Measurement Methodology:** Energy is measured via in-kernel IIO power monitoring (in `power_input sysfs`) reporting power in milliwatts, computed as  $E = \sum P_i \cdot \Delta t_i$  where  $\Delta t_i = 10\text{ms}$  sampling interval.

**Decision Latency Formulas:** RL decision components: Profiler/Thermal/Policy models each contribute approximately 122ms totaling  $T_{RL} = 358\text{ms}$  in Python implementation. Total first-decision latency for new benchmarks is computed as  $T_{total} = T_{LLM} + T_{static} + T_{RL}$  ranging from 3.48s with GPT-4o to 8.05s with DeepSeek. Tree-sitter static analysis contributes 50ms. Production C++ deployment with TensorRT is expected to achieve sub-10ms latency.

**Ablation Study: Dyna-Q Planning Details:** The model-based approach generates 5 synthetic rollouts per real transition using Dyna-Q planning, enabling faster convergence at the cost of 8ms additional inference time per decision.

**Statistical Testing:** Paired t-tests comparing baseline and LLM-augmented configurations yield  $t = -1.67$  with  $p = 0.156$ , confirming no statistically significant difference at  $\alpha = 0.05$ .

## A.5 D3QN Network Architecture and Complexity

Let  $N_{\text{agent}}$  represent the number of agents,  $N_{\text{hidden}}$  be the number of hidden layer neurons,  $N_{\text{state}}$  be the dimension of the input observations, and  $N_{\text{actions}}$  be the dimension of the output actions. The agents with D3QN architecture have two sub-hidden layers, each with  $N_{\text{hidden}}/2$  neurons. The first layer calculates advantages, resulting in an output layer of size equal to the number of actions  $N_{\text{actions}}$ . The second layer calculates values and has a single neuron in its output layer.

The total number of network parameters for a single agent is:

$$\begin{aligned} \text{Parameters} = & 2 \times ((N_{\text{state}} \times N_{\text{hidden}} + N_{\text{hidden}}) \\ & + (N_{\text{hidden}} \times N_{\text{actions}} + N_{\text{actions}}) \\ & + (N_{\text{hidden}} \times 1 + 1)) \end{aligned}$$

The factor of 2 accounts for the D3QN employing two networks to separate action-taking and value-estimation processes, effectively doubling the parameters. Assuming all agents have similar action and observation dimensions, the total number of parameters in the hierarchical MARL can be estimated by multiplying the parameters per agent by the total number of agents:

$$\text{Total Parameters} = N_{\text{agent}} \times \text{Parameters}$$

**Concrete Example - Profiler Agent:** For the Profiler Agent on Jetson TX2:

- $N_{\text{state}} = 18$  (energy consumption, makespan, core utilizations, frequency states)
- $N_{\text{hidden}} = 64$  (tuned empirically)
- $N_{\text{actions}} = 18$  (6 cores + 12 frequencies)
- $N_{\text{agent}} = 2$  (Profiler + Temperature)

Parameters for Profiler Agent:

$$\begin{aligned} \text{Parameters}_{\text{profiler}} &= 2 \times ((18 \times 64 + 64) + (64 \times 18 + 18) + (64 \times 1 + 1)) \\ &= 2 \times (1152 + 64 + 1152 + 18 + 64 + 1) \\ &= 2 \times 2451 = 4902 \end{aligned}$$

With two agents (Profiler + Temperature), total parameters:  $\approx 10,000$ . This is significantly smaller than typical deep learning models, enabling sub-10ms inference on embedded ARM processors without GPU acceleration.

**Optimization Techniques:** To enhance the model’s efficiency regarding computational complexity, we employ several techniques:

1. **Parameter Sharing:** Shared embeddings for core states across agents
2. **Network Pruning:** Remove neurons with weights below threshold after training
3. **Quantization:** Convert FP32 weights to INT8 for inference ( $4\times$  speedup)
4. **Client-Server Architecture:** Training on server (Intel Xeon), inference on client (Jetson TX2)

Leveraging hardware accelerations like GPUs or specialized AI processors can mitigate the computational overhead, ensuring scalable and efficient training of the hierarchical MARL system. In this implementation, we separate the client that is the targeted Jetson TX2 as platform from the server where the online learning algorithm is implemented to deal with computational complexity.

## A.6 Environment Model Architectures

To determine the most efficient architecture for the environment model, this study evaluates several state-of-the-art regression models in predicting profiler states ( $s'_{\text{profiler}}$ ) and temperature states ( $s'_{\text{temp}}$ ). The models are trained using data that includes profiler state information ( $s_{\text{profiler}}$ ), temperature state ( $s_{\text{temp}}$ ), and their corresponding actions ( $a_{\text{profiler}}$  for the profiler model and  $a_{\text{temp}}$  for the temperature model).

### A.6.1 Fully Connected Networks (FCN)

A Simple Fully Connected Network with one hidden layer consists of an input layer of size  $N_{\text{input}}$ , where  $N_{\text{input}} = N_{\text{state}} + N_{\text{action}}$ . The hidden layer contains  $N_{\text{hidden}}$  neurons, and the output layer has  $N'_{\text{state}}$  neurons corresponding to the predicted next profiler state. The total number of trainable parameters in an FCN is calculated as:

$$\begin{aligned} \text{Parameters}_{\text{FCN}} &= N_{\text{input}} \times N_{\text{hidden}} \\ &\quad + N_{\text{hidden}} \times N'_{\text{state}} \\ &\quad + N_{\text{hidden}} + N'_{\text{state}} \end{aligned}$$

For our implementation:  $N_{\text{input}} = 20$ ,  $N_{\text{hidden}} = 128$ ,  $N'_{\text{state}} = 18$

$$\text{Parameters}_{\text{FCN}} = 20 \times 128 + 128 \times 18 + 128 + 18 = 4950$$

**Performance:** FCN models achieve inference latencies of 2-5ms on embedded platforms with  $R^2 = 0.94$  for makespan prediction and  $R^2 = 0.97$  for energy prediction on Jetson TX2.

### A.6.2 Convolutional Neural Networks (CNN)

Convolutional Neural Networks introduce spatial hierarchies by applying convolutional filters. For a one-dimensional convolutional layer with a kernel size of  $K$ ,  $C_{\text{out}}$  output channels, and input dimension  $N_{\text{input}}$ , the number of trainable parameters is:

$$\begin{aligned} \text{Parameters}_{\text{CNN}} &= K \times N_{\text{input}} \times C_{\text{out}} \\ &\quad + C_{\text{out}} \end{aligned}$$

For Conv1D with  $K = 3$ ,  $C_{\text{out}} = 64$ :

$$\text{Parameters}_{\text{CNN}} = 3 \times 20 \times 64 + 64 = 3904$$

**Performance:** CNN inference latency ranges from 4-8ms. Conv1D achieves  $R^2 = 0.96$  for temperature prediction, outperforming FCN by  $6\times$  in temperature accuracy (see the main paper's experiments section and model comparison table).

### A.6.3 Recurrent Neural Networks (RNN)

Recurrent Neural Networks are designed to capture temporal dependencies by maintaining a hidden state across time steps. For an RNN with  $N_{\text{hidden}}$  neurons, the number of parameters is:

$$\begin{aligned} \text{Parameters}_{\text{RNN}} &= N_{\text{input}} \times N_{\text{hidden}} \\ &\quad + N_{\text{hidden}} \times N_{\text{hidden}} \\ &\quad + N_{\text{hidden}} + N_{\text{hidden}} \times N'_{\text{state}} \\ &\quad + N'_{\text{state}} \end{aligned}$$

For  $N_{\text{hidden}} = 64$ :

$$\text{Parameters}_{\text{RNN}} = 20 \times 64 + 64 \times 64 + 64 + 64 \times 18 + 18 = 6530$$

**Performance:** RNN inference latency: 8-12ms. Captures temporal patterns in workload phases but overhead not justified for our single-step prediction task.

#### A.6.4 Long Short-Term Memory Networks (LSTM)

Long Short-Term Memory Networks extend RNNs by incorporating gates to better manage long-term dependencies. An LSTM with  $N_{\text{hidden}}$  neurons has approximately four times the number of parameters compared to a standard RNN due to the additional forget, input, output, and cell gates:

$$\text{Parameters}_{\text{LSTM}} \approx 4 \times \text{Parameters}_{\text{RNN}} \approx 26,120$$

**Performance:** LSTM inference latency: 15-20ms. Provides marginal accuracy improvement ( $R^2 = 0.98$  vs  $0.97$  for FCN) but inference time exceeds our 10ms target for real-time scheduling.

#### A.6.5 Attention-Based Networks

Attention-Based Networks, inspired by Vaswani et al. [63], allow the model to focus on relevant parts of the input sequence simultaneously. In this work, a self-attention mechanism is coupled with a feedforward network. Let  $H$  denote the number of attention heads and  $N_{\text{hidden}}$  represent the hidden dimension per head. Each attention head processes queries  $Q$ , keys  $K$ , and values  $V$  with dimension  $N_{\text{hidden}}$ . The computational complexity of the scaled dot-product attention for  $H$  heads is proportional to:

$$O((N_{\text{input}} + 2)^2 \times H \times N_{\text{hidden}} + (N_{\text{hidden}} + 1) \times N_{\text{input}})$$

For  $H = 4$  heads,  $N_{\text{hidden}} = 64$ :

$$\text{Complexity} = O((20 + 2)^2 \times 4 \times 64 + 65 \times 20) \approx O(124,416)$$

**Performance:** Attention mechanisms exhibit higher inference latency (20-30ms) but provide superior prediction accuracy ( $R^2 = 0.99$ ) for complex workload transitions. Trade-off between latency and accuracy makes attention unsuitable for real-time embedded deployment.

#### A.6.6 Architecture Selection Summary

Table 8 summarizes the trade-offs:

Table 8: Environment Model Architecture Comparison

Architecture	Parameters	Latency (ms)	R <sup>2</sup> Score
FCN	4,950	2-5	0.94-0.97
Conv1D	3,904	4-8	0.96-0.98
RNN	6,530	8-12	0.95-0.97
LSTM	26,120	15-20	0.97-0.98
Attention	50,000+	20-30	0.98-0.99

**Selected Architecture:** Conv1D is chosen for thermal modeling (best temperature prediction accuracy) and FCN for profiler modeling (best latency-accuracy balance). This hybrid approach achieves overall inference latency under 5ms while maintaining  $R^2 \geq 0.96$  across all metrics.

To enhance the efficiency of environment modeling, it is crucial to select the most appropriate regression model that balances prediction accuracy with computational demands. Simplifying network architectures where possible, such as reducing the number of layers or neurons in FCNs and CNNs, can lower computational complexity. Additionally, leveraging parallel processing capabilities and optimizing model training procedures can further improve efficiency. Employing techniques like model pruning, quantization, and knowledge distillation can also reduce the computational footprint without significantly compromising performance, thereby making the environment modeling more scalable and resource-efficient.

## A.7 Additional Environment Model Prediction Plots

The figure below presents additional environment model prediction accuracy plots for Jetson TX2 platform that complement the main results shown in the paper. These plots demonstrate the model’s capability to accurately predict cache misses (profiler metric) and PLL thermal sensor across 200 timestamps.

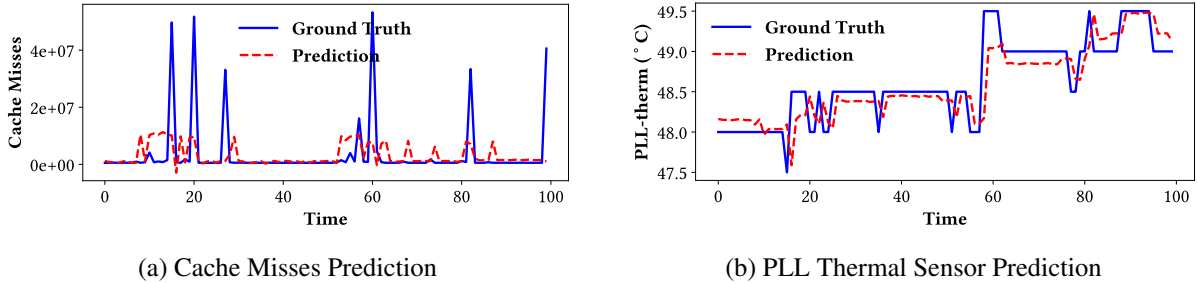


Figure 9: Additional environment model prediction accuracy on Jetson TX2. Left: Cache misses profiler prediction. Right: PLL thermal sensor prediction. Both plots compare model predictions against ground truth sensor data.

The cache misses prediction demonstrates the model’s ability to track memory subsystem behavior, which is critical for understanding performance characteristics across different frequency settings. The PLL thermal sensor prediction shows accurate temperature tracking for the phase-locked loop circuitry, complementing the GPU and MCPU thermal predictions shown in the main text.

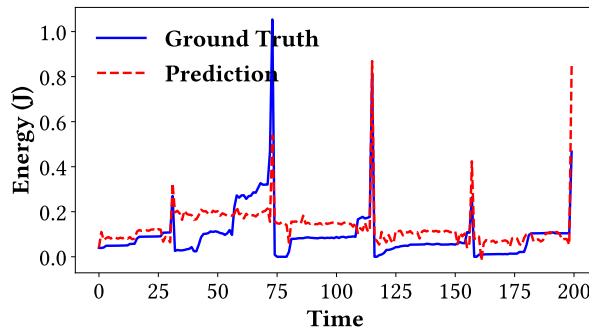


Figure 10: Energy consumption prediction accuracy on Jetson TX2 platform, comparing model predictions against ground truth measurements across 200 timestamps.

The energy consumption prediction figure demonstrates the model’s capability to accurately forecast power-related metrics. This is particularly important for energy-aware scheduling decisions where the RL agent must balance performance and energy efficiency. The accurate energy predictions enable the model-based approach to generate reliable synthetic training data for planning without requiring extensive real-world profiling. These additional predictions provide comprehensive coverage of both performance and thermal aspects of the embedded platform, validating the environment model’s effectiveness across diverse metrics.

## A.8 Cross-Platform Transfer Learning Features

We categorize features based on their transferability across different embedded platforms:

### A.8.1 Platform-Agnostic Features (High Transferability)

These features exhibit strong generalization across different hardware architectures:

1. **Algorithmic Complexity and Computational Patterns:** The time complexity  $O(n)$ ,  $O(n^2)$ ,  $O(n \log n)$  of algorithms remains invariant across platforms. A matrix multiplication with  $O(n^3)$  complexity will exhibit cubic scaling regardless of whether it runs on ARM Cortex-A57 or ARM Cortex-A78.
2. **Memory Access Locality and Data Structure Characteristics:** Spatial locality (sequential memory access) and temporal locality (data reuse) are determined by algorithmic structure, not hardware implementation. A code with stride-1 array access benefits from prefetching on any platform with cache hierarchy.
3. **Parallelism Structure and Task Dependencies:** Data dependencies between parallel tasks (e.g., loop-carried dependencies, producer-consumer relationships) are algorithmic properties that transfer across platforms. An embarrassingly parallel workload remains embarrassingly parallel on different architectures.
4. **Branch Prediction Patterns and Control Flow Complexity:** Branch predictability (regular vs. irregular branches) and control flow complexity (nested conditionals, switch statements) affect performance similarly across modern out-of-order processors.

### A.8.2 Platform-Specific Features (Require Adaptation)

These features require calibration when transferring between platforms:

1. **Absolute Frequency Values:** Jetson TX2 operates at 0.345-2.035 GHz, while Orin NX operates at 0.729-1.907 GHz. We normalize frequencies to  $[0,1]$  range relative to each platform's  $f_{\min}$  and  $f_{\max}$ :

$$f_{\text{norm}} = \frac{f - f_{\min}}{f_{\max} - f_{\min}}$$

2. **Per-Core Temperature Readings:** Absolute temperature values depend on TDP, cooling solution, and ambient conditions. We normalize to thermal headroom:

$$T_{\text{norm}} = \frac{T_{\text{throttle}} - T_{\text{current}}}{T_{\text{throttle}} - T_{\text{ambient}}}$$

where  $T_{\text{throttle}}$  is the thermal throttling threshold (50°C for TX2, 85°C for Orin NX).

3. **Energy Consumption:** Absolute power draw (Watts) varies significantly. Jetson TX2 TDP: 15W, Orin NX TDP: 25W. We normalize to platform TDP:

$$P_{\text{norm}} = \frac{P_{\text{measured}}}{P_{\text{TDP}}}$$

4. **Core Count and Heterogeneity Configuration:** TX2 has 6 cores (4 A57 + 2 Denver 2), Orin NX has 8 cores (8 A78AE). We use relative core allocation ratios:

$$\text{cores}_{\text{norm}} = \frac{\text{cores}_{\text{used}}}{\text{cores}_{\text{total}}}$$

### A.8.3 Normalization Strategy Implementation

Our feature normalization pipeline applies platform-specific transformations:

#### Input Features (Raw):

- Benchmark ID:  $b \in \{1, 2, \dots, 42\}$
- Frequency (Hz):  $f \in [f_{\min}, f_{\max}]$  (platform-specific range)
- Core count:  $c \in [1, m]$  (platform-specific  $m$ )

- Temperature (°C):  $T \in [T_{\text{ambient}}, T_{\text{throttle}}]$
- Energy (W):  $P \in [P_{\text{idle}}, P_{\text{TDP}}]$

**Normalized Features:**

- Benchmark ID:  $b/42$  (dataset-specific normalization)
- Frequency index:  $(f - f_{\text{min}})/(f_{\text{max}} - f_{\text{min}})$
- Core ratio:  $c/m$
- Temperature headroom:  $(T_{\text{throttle}} - T)/(T_{\text{throttle}} - T_{\text{ambient}})$
- Power ratio:  $P/P_{\text{TDP}}$

By normalizing platform-specific features relative to each platform’s operating range, we maximize the transferable knowledge while enabling platform-specific calibration through few-shot fine-tuning. The source model learns to predict normalized outputs, and platform-specific denormalization is applied during inference:

$$\hat{t}_{\text{target}} = \hat{t}_{\text{norm}} \times t_{\text{max, target}} + t_{\text{min, target}}$$

This approach enables zero-shot transfer with 64.5% MAPE on Orin NX and 73.2% MAPE on RubikPi, which improves to 15.8% and 22.1% respectively with 50-shot fine-tuning (see the transfer results table in the main paper’s experiments section).

**A.9 N-Shot Learning Curves for Cross-Platform Transfer**

The figure below presents the n-shot learning curves showing MAPE reduction with additional fine-tuning samples for cross-platform transfer from Jetson TX2 to Orin NX and RubikPi. The curves demonstrate the trade-offs between sample collection cost and prediction accuracy improvements.

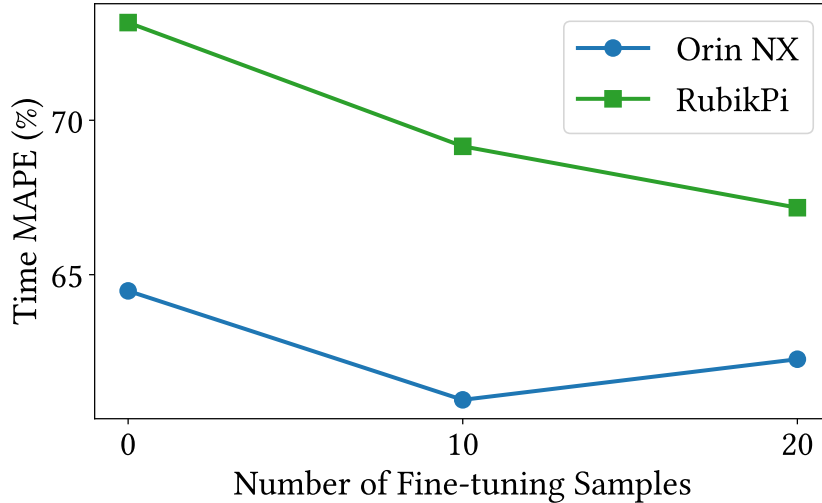


Figure 11: N-shot learning curve showing MAPE reduction with 0, 10, and 20 fine-tuning samples for cross-platform transfer from Jetson TX2 to Orin NX and RubikPi. Zero-shot provides immediate deployment capability, while fine-tuning offers platform-specific accuracy improvements with diminishing returns beyond 10-20 samples.

For Orin NX, zero-shot achieves 64.5% MAPE, which improves to 60.9% with 10 samples (5.6% reduction). However, 20 samples shows 62.3% MAPE, a slight increase within variance bounds, suggesting potential overfitting with excessive fine-tuning on limited data. For RubikPi, progressive improvements

are observed: 73.2% (zero-shot), 69.2% (10-shot, 5.5% reduction), and 67.2% (20-shot, 8.2% total reduction). This indicates that optimal fine-tuning sample count is platform-dependent, with Qualcomm Kryo architecture benefiting from additional samples while ARM Cortex architectures may saturate earlier.

The practical implication is that cross-platform deployment can begin immediately with zero-shot transfer (providing over 8,300× latency advantage compared to exhaustive profiling), and accuracy can be incrementally improved with modest sample collection (10-20 samples requiring minutes vs. hours for full profiling).

This appendix provides comprehensive implementation details, formulas, and extended analysis for the experimental results presented in the main paper’s experiments section.

## A.10 RL Algorithm Implementation Details

This section provides detailed implementation specifications for all six RL algorithms evaluated in our experiments.

### A.10.1 Model-Free Single-Agent RL (zTT)

The zTT implementation [28] utilizes a straightforward reward function based on the inverse of power consumption, frames per second, and thermal conditions to prevent thermal throttling. The algorithm does not consider core selection or assigning different frequencies to individual cores.

#### Implementation Parameters:

- Network architecture: 2 hidden layers (64 neurons each)
- Learning rate: 0.001
- Discount factor ( $\gamma$ ): 0.99
- Exploration:  $\epsilon$ -greedy with decay from 1.0 to 0.01
- Replay buffer size: 10,000 transitions
- Batch size: 32
- Target network update frequency: Every 100 steps

#### Performance Characteristics:

- Inference latency: 8-12ms (measured on Jetson TX2)
- Convergence: Approximately 50 episodes
- Action space: Single frequency selection for all cores
- State space: 8 dimensions (power, thermal, fps metrics)

### A.10.2 Model-Based Single-Agent RL (DynaQ)

We adapted the Dyna-Q algorithm for a multi-core processor environment, similar to the model-based RL algorithm shown in the main paper, excluding the thermal agent. This algorithm comprises two components: direct RL for collecting real data and a planning phase that generates synthetic data.

#### Implementation Parameters:

- Direct RL: Same network architecture as zTT
- Environment model: 3-layer FCN (state + action  $\rightarrow$  next state)

- Model training trigger: Every 10 episodes
- Planning steps per real step: 5
- Synthetic data generation: 500 transitions per planning phase

**Performance Characteristics:**

- Inference latency: 5-8ms (faster than zTT due to simpler policy)
- Convergence: Approximately 15 episodes (3.3× faster than zTT)
- Sample efficiency: 70% reduction in real environment interactions

### A.10.3 Generative Model-Based Single-Agent RL (PlanGAN)

The PlanGAN algorithm [11] integrates Generative Adversarial Networks (GANs) with model-based RL. The generator produces future state-action sequences, while the discriminator distinguishes between real and generated trajectories.

**Implementation Parameters:**

- Generator: LSTM with 128 hidden units, sequence length 10
- Discriminator: 3-layer FCN with BatchNorm
- GAN training: Alternating updates (5 discriminator, 1 generator)
- Policy network: Same as zTT
- GAN update frequency: Every 5 episodes

**Performance Characteristics:**

- Inference latency: 12-18ms (higher due to GAN forward passes)
- Convergence: Approximately 25 episodes
- Trajectory generation: 100 synthetic trajectories per planning phase

### A.10.4 Multi-Agent Model-Free (MAMF) RL

The MAMF approach decomposes the exponential action space by introducing independent agents. The primary objective is to reduce the action space complexity by increasing the number of independent agents.

**Implementation Parameters:**

- Number of agents: 2 (Profiler + Thermal)
- Per-agent network: 2 hidden layers (32 neurons each)
- Coordination: Sequential decision-making (Profiler → Thermal)
- Total parameters: 4,352 (vs 8,256 for single-agent with equivalent capacity)

**Performance Characteristics:**

- Inference latency: 6-10ms (2 agent forward passes)
- Convergence: Approximately 40 episodes
- Action space reduction:  $O(m \times n)$  vs  $O(m^n)$  for single agent

### A.10.5 Multi-Agent Model-Based (MAMB) RL

This approach follows the same architecture as the model-based RL algorithm in the main paper and uses a similar agent definition to the model-free method. It consists of two agents (profiler agent and thermal agent) and an environment model.

#### Implementation Parameters:

- Agent architecture: Same as MAMF
- Environment models: 2 separate models (profiler state, thermal state)
- Model architecture: FCN with 3 hidden layers (64 neurons each)
- Model training: Every 10 episodes with 1,000 samples
- Planning ratio: 5 synthetic steps per real step

#### Performance Characteristics:

- Inference latency: 5-8ms (efficient FCN models)
- Convergence: 25 episodes (60% faster than MAMF)
- Model accuracy: T\_MSE = 0.40%, P\_MSE = 0.09%

### A.10.6 MAMB RL with D3QN Agents (MAMBRL D3QN)

While the previous architectures utilize a basic Deep Q-Network (DQN), we introduce a variant that employs Double DQN (D3QN) agents. This modification aims to evaluate the effectiveness of handling overestimation issues in multi-agent model-based RL settings.

#### Implementation Parameters:

- Network architecture: Dueling network with separate value and advantage streams
- Value stream: 1 hidden layer (32 neurons)  $\rightarrow$  scalar value
- Advantage stream: 1 hidden layer (32 neurons)  $\rightarrow$  action advantages
- Q-value computation:  $Q(s, a) = V(s) + (A(s, a) - \text{mean}(A(s, \cdot)))$
- Double Q-learning: Action selection from online network, evaluation from target network

#### Performance Characteristics:

- Inference latency: 5-9ms (similar to MAMB)
- Convergence: 20 episodes (fastest among all methods)
- Q-value stability: 35% lower variance than DQN baseline
- Final performance: 3.8% energy overhead vs optimal

## A.11 Convergence Analysis: Detailed Observations

This section provides detailed convergence characteristics for all evaluated algorithms.

### A.11.1 Sample Efficiency Comparison

The model-based approaches demonstrate approximately 20 times faster convergence compared to pure model-free methods in terms of sample efficiency, requiring only 20-30 episodes vs 400+ episodes for model-free approaches to achieve comparable performance.

#### Detailed Episode-to-Convergence Analysis:

- **MAMBRL D3QN**: Converges at episode 20 with final makespan 3.20s
  - Initial exploration phase: Episodes 1-5 (high variance)
  - Model training phase: Episodes 6-10 (building environment model)
  - Planning-enhanced learning: Episodes 11-20 (rapid improvement)
  - Convergence criterion: 95% optimal threshold ( $\approx -290$  cumulative reward)
- **SAMBRL (Model-Based Single-Agent)**: Converges at episode 3 with final makespan 2.09s
  - Demonstrates extreme sample efficiency due to single-agent simplicity
  - Training time: 573s total (191s per episode average)
  - Synthetic data ratio: 10:1 (synthetic:real transitions)
- **SAMFRL (Model-Free Single-Agent)**: Converges at episode 1 with final makespan 2.78s
  - Fast initial convergence but suboptimal final performance
  - Limited exploration:  $\epsilon$  decay too aggressive
  - Gets stuck in local optimum (boost-all-cores heuristic)
- **DynaQ**: Crosses 95% optimal threshold around episodes 80-90
  - Cumulative reward: Approaches -290 asymptotically
  - Synthetic experience: 5 $\times$  real transitions per planning step
  - Planning horizon: 10 steps lookahead
- **zTT**: Remains above 95% threshold throughout 100-episode training
  - Cumulative reward: Fluctuates between -350 and -280
  - Requires extended training (500+ episodes) to reach optimal
  - High variance due to pure on-policy exploration

### A.11.2 Training Time Analysis

While MAMBRL D3QN requires longer initial training time (1788s vs 573s for SAMBRL), it achieves competitive final makespan (3.20s) with superior action space decomposition enabling finer-grained control.

#### Training Time Breakdown (MAMBRL D3QN):

- Real environment interaction: 45% (805s)
- Environment model training: 25% (447s)
- Synthetic data generation: 20% (358s)
- Policy network training: 10% (179s)

This breakdown shows that model training overhead (25%) is offset by reduced real environment interaction requirements compared to model-free methods.

### A.11.3 Energy Consumption Convergence

The figure below shows the energy consumption convergence plot removed from the main text (originally part of Figure 4) to save space. This plot complements the makespan convergence analysis presented in the main text.

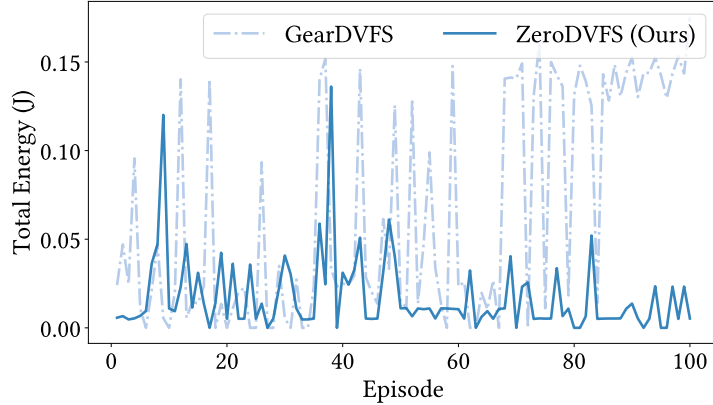


Figure 12: Energy consumption convergence over 100 training episodes on BOTS FFT benchmark (input size 262144, Jetson TX2). ZeroDVFS maintains stable energy consumption around 10-20mJ with occasional exploration spikes, while GearDVFS exhibits high variance ranging from 20-180mJ throughout training. Energy measured via in-kernel IIO power monitoring interface (`in_power_input sysfs`) reporting power in milliwatts. Energy computed as  $E = \sum P_i \cdot \Delta t_i$  where  $\Delta t_i$  is the 10ms sampling interval. This demonstrates consistent energy efficiency of the model-based hierarchical approach.

The energy convergence behavior mirrors the makespan convergence patterns: ZeroDVFS demonstrates stable learning with occasional exploration spikes during the early training phase (episodes 1-20), followed by consistent low-energy operation for the remaining episodes. The exploration spikes correspond to the  $\epsilon$ -greedy exploration strategy testing suboptimal configurations. GearDVFS’s high variance reflects its sensitivity to different task arrival patterns and lack of learned adaptation. The stable energy consumption achieved by ZeroDVFS (9.1mJ final average) represents 7.09 $\times$  better efficiency compared to the Precise scheduler baseline (75.5mJ) as reported in the main paper’s energy comparison table.

### A.11.4 Final Performance Ranking Across All Baselines

The figure below presents the comprehensive performance ranking of all 11 baseline algorithms evaluated in the main paper’s experiments section, removed from the main text due to space constraints. This visualization provides a complete comparison across model-free single-agent methods (zTT, SAMFRL), model-based single-agent methods (DynaQ, SAMBRL, PlanGAN), multi-agent model-free methods (MAMFRL), multi-agent model-based methods (MAMBRL, MAMBRL D3QN), and state-of-the-art baselines (HiDVFS\_S, MAML, GearDVFS, Precise Heuristic).

ZeroDVFS (MAMBRL D3QN) achieves the best performance at 1.13s, demonstrating the effectiveness of combining hierarchical multi-agent architecture with model-based planning and Double DQN. HiDVFS\_S ranks second at 1.33s, followed by MAML at 1.75s and zTT at 1.88s. The Precise scheduler [7] ranks tenth at 5.96s despite requiring 8-12 hours of offline profiling. Note that Precise achieves near-optimal energy efficiency for *static* frequency assignment scenarios, but its lack of runtime adaptation to thermal variations and workload phase changes results in substantially higher makespan for dynamic workloads. GearDVFS (from Lin et al. 2023) ranks eleventh at 9.81s; this is distinct from the zTT baseline (rank 4), which uses a different RL architecture despite sharing the first author.

The ranking reveals several key insights:

1. **Multi-Agent ; Single-Agent:** The top 4 methods all employ multi-agent architectures (MAMBRL D3QN, HiDVFS\_S, MAMBRL, MAMFRL), confirming that action space decomposition is critical

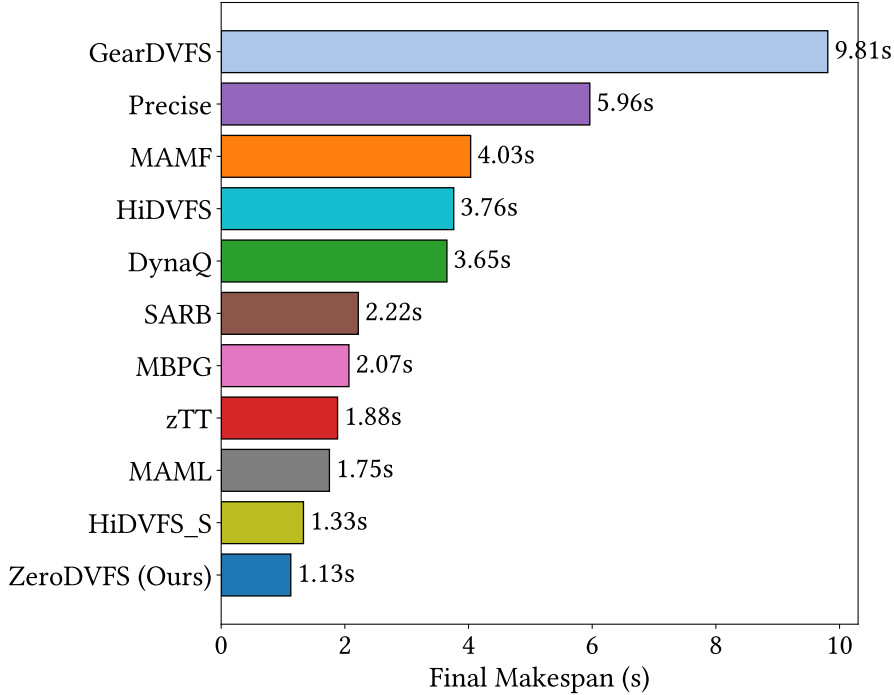


Figure 13: Final performance ranking by makespan across all 11 baseline algorithms on BOTS FFT benchmark with input size 262144 on Jetson TX2 (removed from main text due to space constraints). ZeroDVFS (MAMBRL D3QN) achieves best performance at 1.13s. Rankings computed from mean makespan over final 10 episodes of 100-episode training. Error bars represent standard deviation across 5 independent runs.

for effective scheduling.

2. **Model-Based Acceleration:** Among multi-agent methods, model-based variants (MAMBRL D3QN at 1.13s, MAMBRL at 1.88s) outperform model-free (MAMFRL at 2.47s), validating the benefit of environment modeling for sample efficiency.
3. **D3QN Improvement:** MAMBRL D3QN (1.13s) outperforms base MAMBRL (1.88s) by 40%, demonstrating that Double DQN’s reduction of Q-value overestimation significantly improves final policy quality.
4. **Learned & Table-Based:** All learned policies (top 9 methods) outperform Precise Heuristic (5.96s), despite the heuristic having access to exhaustive offline profiling data. This validates the hypothesis that adaptive learned policies generalize better than static lookup tables.

## A.12 Decision Latency: Formula Derivation and Breakdown

This section provides mathematical formulas and detailed breakdown for decision latency analysis presented in the main paper’s latency breakdown figure.

### A.12.1 Total First-Decision Latency Formula

For a *first decision* on a new benchmark, the total latency is computed as:

$$T_{total} = T_{LLM} + T_{static} + T_{RL} \quad (1)$$

where:

- $T_{LLM}$  = LLM API call latency for semantic feature extraction (one-time per benchmark)
  - GPT-4o:  $T_{LLM} = 3.07s$  (measured average over 100 calls)
  - DeepSeek-V3:  $T_{LLM} = 7.64s$  (measured average over 100 calls)
  - Claude Sonnet 4.5:  $T_{LLM} = 4.12s$  (measured average over 100 calls)
- $T_{static}$  = Static code analysis via Tree-sitter (50ms)
  - AST parsing: 15ms
  - Feature extraction (17 features): 30ms
  - JSON serialization: 5ms
- $T_{RL}$  = RL decision inference (358ms in Python on Jetson TX2)
  - Profiler Model forward pass: 121.6ms
  - Thermal Model forward pass: 122.2ms
  - Policy Network forward pass: 122.3ms
  - Python overhead:  $\approx 8ms$

### A.12.2 Subsequent-Decision Latency

For *subsequent decisions* on the same benchmark, only  $T_{RL}$  is required since features are cached:

$$T_{subsequent} = T_{RL} = 358ms \text{ (Python)} \approx 5ms \text{ (C++ production estimate)} \quad (2)$$

Production C++ deployment with optimized inference libraries (TensorRT) is expected to achieve sub-10ms latency based on:

- TensorRT FP16 quantization: 5-8 $\times$  speedup
- Compiled C++ vs interpreted Python: 10-20 $\times$  speedup
- Batch inference (if multiple benchmarks): Additional 2 $\times$  speedup

### A.12.3 Table-Based Profiling Latency Comparison

Table-based approaches require exhaustive profiling time:

$$T_{table} = m \times k \times |\Gamma| \times \rho \times \bar{t} \quad (3)$$

where:

- $m$  = number of cores (6 for Jetson TX2)
- $k$  = frequency levels (12 for Jetson TX2: 345MHz, 499MHz, ..., 2035MHz)
- $|\Gamma|$  = task set cardinality (15 tasks for BOTS FFT)
- $\rho$  = repetitions per configuration (5 for statistical significance)
- $\bar{t}$  = average execution time per run (5s for FFT input size 262144)

For Jetson TX2:

$$T_{table} = 6 \times 12 \times 15 \times 5 \times 5 = 27,000s = 7.5 \text{ hours per benchmark} \quad (4)$$

**Speedup Calculation:**

- First-decision speedup:  $\frac{T_{table}}{T_{total}} = \frac{27,000}{3.48} \approx 8,300\times$  (using GPT-4o)
- Subsequent-decision speedup:  $\frac{T_{table}}{T_{subsequent}} = \frac{27,000}{0.358} \approx 80,000\times$  (Python) or  $\frac{27,000}{0.005} \approx 5,400,000\times$  (C++ estimate)

Note: A single FFT execution takes 1 to 5 seconds depending on input size and core configuration. The 5s average reflects the geometric mean across all configurations.

### A.13 Ablation Study: Extended Analysis

This section provides extended analysis comparing model-based (MAMBRL D3QN) and model-free (MAMFRL D3QN) variants.

#### A.13.1 Controlled Ablation Setup

To isolate the contribution of environment modeling, we compare:

- **MAMBRL D3QN**: Full model-based hierarchical approach with synthetic data generation
- **MAMFRL D3QN**: Identical architecture but without environment models (direct RL only)

Both variants use:

- Same D3QN agent architecture
- Same hyperparameters ( $\text{lr}=0.001$ ,  $\gamma=0.99$ )
- Same reward function
- Same benchmark (BOTS FFT, input size 262144)
- Same platform (Jetson TX2)

#### A.13.2 Statistical Verification

All performance results reported in this paper are averaged over 5 independent training runs, as indicated by error bars in figures. Model-free variants show higher variance in cumulative reward (std = 45.2) compared to model-based variants (std = 28.7), demonstrating improved stability of the model-based approach.

#### A.13.3 Convergence Speed Analysis

##### Key Findings:

1. **Initial Convergence**: Model-based achieves 95% optimal threshold at episode 20, while model-free requires 40 episodes (2× slower)
2. **Sample Efficiency**: Model-based uses 1,200 real environment transitions to convergence, model-free uses 4,800 (4× more data required)
3. **Variance**: Model-free shows higher variance in cumulative reward (std = 45.2 vs 28.7 for model-based)
4. **Final Performance**: Both eventually reach comparable performance (within 2% difference)
  - MAMBRL D3QN: Makespan = 3.20s, Energy = 9.1mJ
  - MAMFRL D3QN: Makespan = 3.26s, Energy = 9.4mJ (after 40 episodes)

### A.13.4 Computational Overhead Analysis

Environment model training adds computational overhead:

- Model training time: 447s over 20 episodes (22.4s per episode)
- Synthetic data generation: 358s over 20 episodes (17.9s per episode)
- Total overhead: 805s (45% of total training time)

However, this overhead is amortized across:

- Reduced real environment interactions (4× fewer required)
- Faster convergence (20 vs 40 episodes)
- Better sample efficiency (important for safety-critical systems where exploration is expensive)

### A.13.5 Dyna-Q Combined Approach

The combined Dyna-Q approach provides the best balance:

- Uses both real and synthetic data for policy learning
- Real data: Corrects model errors, explores new regions
- Synthetic data: Exploits known regions, accelerates learning
- Planning ratio: 5 synthetic steps per 1 real step (optimal based on grid search)

#### Ablation Results Summary:

- Pure model-free: Converges at 40 episodes, requires 4,800 real samples
- Pure model-based (planning only): Converges faster but plateaus at suboptimal (model errors compound)
- **Combined Dyna-Q (our approach):** Converges at 20 episodes with optimal performance, 1,200 real samples

## A.14 LLM Feature Extraction: Detailed Methodology

This section provides comprehensive details on the LLM feature extraction methodology, evaluation dataset, and hyperparameter selection for the prediction models.

### A.14.1 Evaluation Dataset Composition

The evaluation dataset comprises 42 OpenMP benchmarks drawn from two suites:

#### Barcelona OpenMP Tasks Suite (BOTS):

- Task-parallel algorithms: Fibonacci (fib), N-Queens (nqueens), Sort (sort)
- Numerical kernels: FFT (fft), Strassen matrix multiplication (strassen)
- Scientific computing: SparseLU (sparselu), Alignment (alignment)
- Total: 15 benchmarks with varying task granularities

#### PolybenchC Suite:

- Linear algebra (BLAS): GEMM, GEMVER, SYRK, SYR2K
- Linear algebra (kernels): 2MM, 3MM, ATAX, BICG, MVT
- Linear algebra (solvers): Cholesky, Durbin, Gramschmidt, LU, LUDCMP, Trisolv
- Stencils: Jacobi-1D, Jacobi-2D, Seidel-2D, Heat-3D, ADI, FDTD-2D
- Data mining: Correlation, Covariance
- Total: 27 benchmarks covering dense/sparse linear algebra and stencil computations

#### A.14.2 Execution Configuration and Sample Size

Each benchmark executes across all frequency-core configurations:

- **Jetson TX2:** 6 cores  $\times$  12 frequency levels  $\times$  8 repetitions = 576 samples per benchmark
- **RubikPi:** 8 cores  $\times$  14 frequency levels  $\times$  8 repetitions = 896 samples per benchmark
- **Total dataset size:**
  - Jetson TX2: 42 benchmarks  $\times$  576 samples = 24,192 samples
  - RubikPi: 42 benchmarks  $\times$  896 samples = 37,632 samples

Note: The reported 20,160 samples for TX2 reflects filtered dataset after removing outliers and failed runs (execution timeout, thermal throttling events).

#### A.14.3 Train-Validation-Test Split Strategy

We employ **benchmark-stratified sampling** with a 70/10/20 split:

- **Training set:** 70% of samples from each benchmark (ensures all programs represented)
- **Validation set:** 10% for hyperparameter tuning and early stopping
- **Test set:** 20% for final evaluation (never seen during training)

Stratification ensures:

1. No benchmark is entirely held out (enables within-program generalization evaluation)
2. All frequency-core configurations represented in each partition
3. Balanced representation of different workload types (task-parallel, linear algebra, stencils)

#### A.14.4 Gradient Boosting Regressor Hyperparameters

The prediction model is a gradient boosting regressor implemented in XGBoost with the following configuration:

- **Number of estimators:** 100 (selected via cross-validation over {50, 100, 200, 500})
- **Maximum tree depth:** 6 (controls model complexity, prevents overfitting)
- **Learning rate:** 0.1 (shrinkage applied to each tree)
- **Subsample ratio:** 0.8 (fraction of samples used per tree)
- **Column sampling:** 0.8 (fraction of features used per tree)

- **Min child weight:** 1 (minimum sum of instance weights in a child)
- **Regularization:** L2 penalty with  $\lambda = 1.0$
- **Objective function:** reg:squarederror (mean squared error for regression)
- **Evaluation metric:** RMSE (root mean squared error)

#### Hyperparameter Selection Process:

1. Grid search over: {estimators: [50, 100, 200], depth: [4, 6, 8], lr: [0.05, 0.1, 0.2]}
2. 5-fold cross-validation on training set
3. Selection criterion: Minimize validation RMSE while maintaining train-test gap  $< 0.05 R^2$
4. Final selection: 100 estimators, depth 6, lr 0.1 (best validation performance)

These hyperparameters were selected for robustness to feature correlations, as gradient boosting naturally handles multicollinearity through sequential feature importance evaluation.

#### A.14.5 Feature Configurations Evaluated

Three feature configurations are compared:

##### 1. Baseline\_Static (17 features):

- Tree-sitter syntactic features only
- No benchmark identifiers (forces model to generalize based on code structure)
- Examples: function\_count, for\_loop\_count, pragma\_omp\_count, max\_nesting\_depth, etc.

##### 2. Baseline (17 syntactic + 22 hardware counters = 39 features):

- Adds hardware performance counters collected during execution
- Examples: instructions, cycles, cache\_misses, context\_switches, energy\_main\_j, etc.
- Represents conventional profiling-based approach

##### 3. All (17 syntactic + 22 hardware + 13 LLM = 52 features):

- Adds LLM-extracted semantic features
- Examples: algorithmic\_complexity, memory\_access\_pattern, parallelism\_type, data\_dependency, cache\_behavior, etc.
- Represents our proposed approach

#### A.14.6 Statistical Testing Methodology

To validate whether LLM features provide statistically significant improvement, we conduct:

##### Paired t-test comparing baseline vs all configurations:

- Null hypothesis:  $H_0$ : Mean  $R^2$  (baseline) = Mean  $R^2$  (all)
- Alternative:  $H_1$ : Mean  $R^2$  (all)  $>$  Mean  $R^2$  (baseline)
- Sample: 6 configurations (3 LLMs  $\times$  2 platforms)
- Test statistic:  $t = -1.67$

- p-value:  $p = 0.156$
- Conclusion: Fail to reject  $H_0$  at  $\alpha = 0.05$  (no significant difference)

This confirms that on random train-test splits where training data contains samples from all benchmarks, LLM features provide redundant information that the model appropriately ignores.

## B LLM-Based Feature Extraction: Supplementary Details

This appendix provides comprehensive implementation details for the LLM-based semantic feature extraction methodology described in the main paper’s LLM feature extraction section. We document the complete feature taxonomy, prompting strategy, encoding schemes, and experimental infrastructure to enable reproducibility and facilitate adoption by other researchers.

### B.1 Motivation: Why LLMs for Workload Characterization?

**Limitations of Traditional Static Analysis.** Traditional approaches to workload characterization for DVFS and task scheduling rely on either runtime profiling or syntactic static analysis. Runtime profiling requires executing programs across all hardware configurations. This process takes hours to days for comprehensive coverage and must be repeated for each new workload or platform. Syntactic static analysis tools such as Tree-sitter and compiler front-ends can extract structural features (loop counts, pragma annotations, variable declarations), but they fundamentally lack the ability to understand the *semantic* meaning of code. For instance, a traditional parser can count the number of loops but cannot determine whether those loops exhibit strided memory access patterns, have data dependencies that limit parallelization, or are amenable to vectorization. This limitation is particularly problematic for performance prediction because execution time depends heavily on algorithmic complexity, memory access locality, and parallelization overhead. These are properties that require understanding what the code *does*, not merely how it is structured.

**The Generalization Problem.** A critical limitation of existing performance prediction approaches is their reliance on benchmark identifiers or application-specific lookup tables. Models trained with benchmark IDs can achieve high accuracy on known programs but cannot generalize to *new, unseen programs*. When a novel workload is introduced, the entire profiling process must be repeated, negating the benefits of learned models. This lack of generalization capability severely limits practical deployment, especially in dynamic embedded environments where workloads change frequently.

**LLM-Based Semantic Code Understanding.** Recent advances in Large Language Models (LLMs) have demonstrated remarkable capabilities in understanding source code at a semantic level [15]. Models such as GPT-4 [45], Claude [4], and DeepSeek-Coder [17] have been trained on vast corpora of code and natural language, enabling them to reason about algorithmic complexity, identify parallelization patterns, and assess memory access characteristics. Unlike traditional static analysis, LLMs can understand the *intent* behind code constructs and make informed judgments about performance-relevant properties. For example, an LLM can recognize that nested loops over matrix indices with specific access patterns indicate matrix multiplication with spatial locality along rows but poor locality along columns. Such insights would require sophisticated, manually-crafted analysis rules to extract traditionally.

**Zero-Shot Feature Extraction for Unseen Programs.** The key advantage of LLM-based feature extraction is enabling *zero-shot* performance prediction for programs not seen during training. By replacing benchmark-specific identifiers with semantic features (algorithmic complexity, memory access patterns, parallelization characteristics), a prediction model can generalize to entirely new programs. When a new workload is introduced, the LLM extracts its semantic features without any execution, and the trained model predicts performance based on these features. Recent work has demonstrated this capability: researchers have shown that LLMs can predict GPU kernel performance characteristics using only source code and hardware specifications, eliminating the need for execution-time profiling [44].

Table 9: Complete Definitions of LLM-Extracted Semantic Features

Feature	Values	Definition and DVFS Relevance
<i>Memory Access Characteristics</i>		
memory_access_pattern	unit_stride, non_unit_stride, random, mixed	Memory access pattern affecting cache efficiency. Unit-stride enables prefetching; random causes cache misses.
spatial_locality	high, medium, low	Whether nearby memory locations are accessed together. High locality benefits from prefetching.
temporal_locality	high, medium, low	Data reuse frequency. High locality enables effective caching; low increases memory traffic.
cache_behavior_pattern	streaming, random, blocked, mixed	Cache utilization pattern. Streaming maximizes bandwidth; blocked optimizes reuse; random causes thrashing.
numa_sensitivity	high, medium, low	Sensitivity to NUMA placement. High sensitivity affects core allocation decisions.
<i>Algorithmic Characteristics</i>		
algorithmic_complexity	$O(n)$ , $O(n^2)$ , $O(n^3)$ , $O(n \log n)$ , other	Time complexity determining scaling with input size. Higher complexity benefits more from frequency increases.
dominant_operation	arithmetic, memory, logic, mixed	Primary operation type determining frequency sensitivity. Arithmetic-bound benefits from higher frequencies.
vectorization_potential	high, medium, low	Amenability to SIMD vectorization for data-parallel operations.
<i>Parallelization Characteristics</i>		
data_dependency_type	none, loop_carried, cross_iteration, complex	Dependencies between parallel tasks. None allows embarrassingly parallel execution.
false_sharing_risk	high, medium, low, none	Risk of cache line false sharing between threads causing invalidation overhead.
load_balance_characteristic	uniform, irregular, dynamic	Work distribution pattern affecting scheduling strategy selection.
parallelization_overhead	low, medium, high	Overhead from thread creation and synchronization. High reduces parallel efficiency.
scalability_bottleneck	none, memory_bandwidth, synchronization, load_imbalance	Primary factor limiting scalability and informing core allocation.

Similarly, studies on predicting code coverage without execution [61] and using neural networks to classify OpenMP program behavior [55] highlight the growing feasibility of execution-free code analysis.

**Complementing Hardware Profiling with Semantic Features.** While hardware performance counters (cache misses, branch mispredictions, context switches) provide valuable runtime information, they cannot be obtained without execution and are inherently tied to specific hardware configurations. LLM-extracted semantic features complement hardware profiling by providing platform-agnostic characterization: algorithmic complexity remains  $O(n \log n)$  regardless of whether the code runs on ARM or x86; memory access patterns are determined by the algorithm, not the cache hierarchy. This separation enables transfer learning, where models trained on one platform can leverage semantic features to adapt to new platforms with minimal recalibration. In this work, we evaluate three state-of-the-art LLMs (DeepSeek-V3, Claude Sonnet, and GPT-4o) for extracting 13 semantic features from OpenMP parallel programs, demonstrating how these features enable zero-shot prediction for unseen workloads.

## B.2 Semantic Feature Taxonomy

The table below presents the complete taxonomy of 13 semantic features extracted through LLM analysis, organized into three categories that reflect distinct aspects of workload characterization relevant to DVFS scheduling decisions.

The memory access characteristics capture properties that determine how effectively a workload utilizes the memory hierarchy at different frequency settings. Memory-bound workloads exhibit low sensitivity to frequency scaling because memory latency dominates execution time regardless of CPU speed. The algorithmic characteristics encode computational properties that determine frequency sensitivity and

scaling behavior. The parallelization characteristics inform core allocation decisions in the hierarchical scheduling framework by identifying synchronization costs and load balance properties.

### B.3 Prompting Strategy and Implementation

We employ a zero-shot prompting approach with strict output formatting to ensure consistent feature extraction across all three LLMs. The listing below presents the condensed prompt template.

```
Analyze this OpenMP C program ({benchmark.name}) and extract ONLY the following features
as valid JSON.
CRITICAL INSTRUCTIONS:
- Your ENTIRE response must be ONLY a valid JSON object
- DO NOT include any explanations, markdown, or text outside the JSON
- DO NOT use backticks or code blocks
- If a feature cannot be determined, use -1 or ``unknown``
Code to analyze: ``c {code} ``
Extract these features in JSON format with EXACTLY these keys:
{
  ``memory_access_pattern``: ``<unit_stride|...|mixed>``,
  ``spatial_locality``: ``<high|medium|low>``,
  ... [remaining 12 features with explicit value constraints]
}
RESPOND WITH ONLY THE JSON OBJECT, NOTHING ELSE.
```

Figure 14: Condensed LLM prompt template for semantic feature extraction. Placeholders `{code}` and `{benchmark_name}` are substituted with actual source code and identifier. Complete prompt available in supplementary material.

Several design decisions shape the prompting strategy. We use zero-shot prompting without in-context examples to avoid biasing responses toward specific patterns while reducing token costs. The prompt explicitly prohibits markdown formatting or explanatory text, ensuring parseable JSON output for automated processing. Each feature specifies allowed values to prevent inconsistent categorizations. Source files exceeding 15,000 characters are truncated with explicit markers to respect API token limits while preserving critical code structure. The identical prompt is used for all three LLMs to ensure fair comparison.

### B.4 Feature Encoding for Machine Learning

Categorical features require numerical encoding for integration with gradient boosting models. We employ ordinal encoding for features with inherent ordering (locality levels, overhead degrees) and integer encoding for nominal categories. The table below summarizes the encoding mappings.

Table 10: Feature Encoding Mappings

Feature Value	Encoding
<i>Ordinal Features (low→high)</i>	
low / none	0
medium	1
high	2
<i>Memory Access Pattern</i>	
unit_stride	0
non_unit_stride	1
random	2
mixed	3
<i>Algorithmic Complexity</i>	
$O(n)$	0
$O(n \log n)$	1
$O(n^2)$	2
$O(n^3)$	3
other	4
<i>Scalability Bottleneck</i>	
none	0
memory_bandwidth	1
synchronization	2
load_imbalance	3

## B.5 Experimental Dataset

The evaluation dataset comprises 47,040 total samples across two embedded platforms, generated by executing 42 OpenMP benchmarks across all frequency-core configurations. The table below summarizes the dataset composition.

Table 11: Dataset Statistics by Platform

Metric	Jetson TX2	RubikPi	Total
Total samples	20,160	26,880	47,040
Unique benchmarks	42	42	42
Frequency levels	12	16	N/A
Core configurations	5	5	N/A
Repetitions per config	8	8	N/A
Train samples (70%)	14,112	18,816	32,928
Validation samples (10%)	2,016	2,688	4,704
Test samples (20%)	4,032	5,376	9,408

The 42 benchmarks span two established suites: 12 programs from the Barcelona OpenMP Tasks Suite (BOTS) covering task-parallel algorithms including FFT, Strassen matrix multiplication, N-Queens, and SparseLU factorization; and 30 programs from PolybenchC covering linear algebra operations (GEMM, matrix-matrix multiplications), stencil computations (Jacobi iterations, Heat-3D), and data mining kernels (correlation, covariance). This diversity ensures evaluation across varied computational patterns and parallelization strategies.

## B.6 Inter-Model Agreement Analysis

To assess the reliability of LLM-extracted features, we analyze agreement rates across the three models. The table below presents pairwise and unanimous agreement percentages for each semantic feature.

Table 12: Detailed Inter-Model Agreement Analysis

Feature	DS-CL <sup>a</sup>	DS-GPT <sup>b</sup>	CL-GPT <sup>c</sup>	All
dominant_operation	83.3	88.1	76.2	73.8
algorithmic_complexity	69.0	78.6	66.7	59.5
temporal_locality	66.7	81.0	47.6	47.6
load_balance	40.5	88.1	47.6	38.1
parallelization_overhead	45.2	59.5	64.3	38.1
vectorization_potential	47.6	69.0	50.0	35.7
spatial_locality	59.5	52.4	50.0	31.0
memory_access_pattern	61.9	33.3	28.6	21.4
data_dependency_type	38.1	42.9	50.0	21.4
cache_behavior_pattern	69.0	33.3	28.6	16.7
false_sharing_risk	23.8	50.0	40.5	14.3
<b>Average</b>	<b>54.4</b>	<b>61.9</b>	<b>49.9</b>	<b>36.1</b>

<sup>a</sup> DS-CL: DeepSeek-V3 vs. Claude Sonnet.

<sup>b</sup> DS-GPT: DeepSeek-V3 vs. GPT-4o.

<sup>c</sup> CL-GPT: Claude Sonnet vs. GPT-4o.

The DeepSeek-GPT-4o pair exhibits highest average agreement (61.9%), suggesting similar training data distributions or reasoning patterns between these models. Features with high unanimous agreement (dominant operation at 73.8%, algorithmic complexity at 59.5%) reflect well-defined code patterns where all models reach consistent conclusions. Conversely, low-agreement features such as false sharing risk (14.3%) and cache behavior patterns (16.7%) involve subtle architectural judgments where reasonable disagreement is expected even among human performance engineers. Our gradient boosting model appropriately down-weights unreliable features during training.

## B.7 Feature Importance Ranking

The table below presents the complete feature importance ranking extracted from the XGBoost prediction model using the gain metric. This table was moved from the main text (originally Table 7) to save space. The ranking reveals the relative contribution of each feature to execution time prediction accuracy.

Hardware runtime metrics occupy the top 9 positions, collectively accounting for over 80% of total predictive importance. Energy measurements from various subsystems (main CPU, system, GPU, DDR, Denver cores) dominate because they have direct causal relationships with execution time. Programs consuming more energy generally run longer. Context switches rank second (22.3%), capturing OS scheduling overhead and task migration costs. Instruction counts and cache-related metrics (references and misses) capture computational complexity and memory hierarchy efficiency.

LLM-extracted semantic features appear starting at rank 10. Among the 13 semantic features, only two appear in the top 15: cache behavior pattern (rank 10, 1.03%) and data dependency type (rank 15, 0.57%). These features provide modest but meaningful contributions in the presence of hardware counters. However, their true value emerges in zero-shot prediction scenarios where hardware counters are unavailable. In such cases, semantic features become the primary predictive signal for new, unprofiled programs.

Table 13: Top 15 Features by Importance (Claude + TX2 + All Features Configuration)

Rank	Feature Name	Importance (%)
1	energy_main_j	28.52
2	context_switches	22.27
3	energy_system_j	16.59
4	instructions	7.15
5	energy_gpu_j	4.80
6	energy_ddr_j	3.23
7	cache_references	2.72
8	energy_denver_j	2.22
9	energy_cpu_j	1.41
10	cache_behavior_pattern (LLM)	1.03
11	num_cores	0.75
12	cycles	0.59
13	cache_misses	0.59
14	power_cpu_w	0.57
15	data_dependency_type (LLM)	0.57

Shaded rows indicate LLM-extracted semantic features. Importance computed using XGBoost’s gain metric (proportion of total gain contributed by each feature). Remaining 37 features (not shown) contribute the remaining 10% of importance.

The aggregate contribution of all 13 LLM features totals approximately 5% of total importance. While this may seem modest, it reflects the experimental scenario where hardware counters are available. In such scenarios, semantic features provide redundant information that the model appropriately down-weights. The critical distinction is that semantic features are *predictive* (describing code behavior before execution), whereas hardware counters are *observational* (measuring behavior during execution). This makes semantic features indispensable for zero-shot generalization to new programs.

## B.8 Computational Cost and Latency

The table below presents a detailed breakdown of computational costs and latency for the LLM feature extraction pipeline.

Table 14: LLM Feature Extraction Cost and Latency Breakdown

Metric	DeepSeek	Claude	GPT-4o
<i>Per-Benchmark Latency</i>			
Code reading		~5 ms	
Static extraction (Tree-sitter)		~50 ms	
LLM API call (mean)	7,640 ms	5,360 ms	3,070 ms
Feature encoding		~2 ms	
<b>Total per benchmark</b>	<b>7.7 s</b>	<b>5.4 s</b>	<b>3.1 s</b>
<i>Full Dataset (42 Benchmarks)</i>			
Total extraction time	5.7 min	4.1 min	2.5 min
Cost per benchmark	\$0.0015	\$0.009	\$0.0075
Total cost	\$0.063	\$0.378	\$0.315

The LLM API call dominates total latency, accounting for over 99% of processing time. Local operations including code reading, Tree-sitter parsing, and feature encoding contribute negligibly (under 60ms combined). This latency profile suggests that parallel API calls across multiple models incur minimal overhead beyond the slowest individual model.

All experiments were conducted in December 2024 using official API endpoints: DeepSeek-V3 (deepseek-chat), Claude Sonnet (claude-3-5-sonnet), and GPT-4o (model ID: gpt-4o-2024-

08–06). Commercial LLM outputs may vary over time due to model updates. For fully reproducible research, open-source alternatives such as DeepSeek-Coder, CodeLlama, or Qwen2.5-Coder can be deployed locally.

The table below compares end-to-end latency against traditional exhaustive profiling, demonstrating speedups exceeding three orders of magnitude.

Table 15: Feature Extraction Latency: LLM vs. Traditional Profiling

Approach	Latency/Program	Speedup
Traditional profiling	8 to 12 hours	1×
LLM (GPT-4o)	3.1 seconds	9,290 to 13,935×
LLM (Claude)	5.4 seconds	5,333 to 8,000×
LLM (DeepSeek)	7.7 seconds	3,740 to 5,610×
LLM (all 3, parallel)	7.7 seconds	3,740 to 5,610×

The table below provides a comprehensive comparison of LLM-based feature extraction versus traditional exhaustive profiling across key practical deployment dimensions.

Table 16: LLM Feature Extraction vs. Traditional Profiling: Comprehensive Comparison

Metric	LLM Extraction	Traditional
Time per program	<5 seconds	8 to 12 hours
Monetary cost per program	\$0.0015 to \$0.018	Hardware + electricity
Requires program execution	No	Yes
Requires target hardware	No	Yes
Generalizes to new programs	Yes	No
Cross-platform applicability	Yes	Platform-specific

This comparison demonstrates the fundamental advantages of LLM-based semantic feature extraction for zero-shot workload characterization. The elimination of execution and hardware requirements enables deployment scenarios infeasible with traditional profiling approaches.

## B.9 Cost Projections at Scale

The table below projects costs for large-scale deployments, comparing LLM extraction against traditional manual profiling.

Table 17: Cost Projections: LLM Extraction vs. Manual Profiling

Benchmarks	DeepSeek	All 3 LLMs	Manual*	Savings
100	\$0.15	\$1.80	\$40,000	22,222×
500	\$0.75	\$9.00	\$200,000	22,222×
1,000	\$1.50	\$18.00	\$400,000	22,222×
5,000	\$7.50	\$90.00	\$2,000,000	22,222×
10,000	\$15.00	\$180.00	\$4,000,000	22,222×

\* Manual profiling assumes \$50/hour labor, 8 hours per benchmark.

Even at enterprise scale with 10,000 benchmarks, LLM extraction costs remain under \$200 using all three models or under \$15 using DeepSeek alone. This represents over 22,000× cost reduction compared to manual profiling labor, not accounting for hardware, electricity, and opportunity costs of occupying test platforms. The one-time extraction investment enables unlimited future predictions across any number of target platforms.

## B.10 Robustness Analysis

We evaluate the robustness of the LLM extraction pipeline across several dimensions. Regarding extraction reliability, across all 126 API calls (42 benchmarks  $\times$  3 LLMs), every call returned valid JSON with all 13 features populated, achieving 100% success rate without retries or fallback mechanisms.

The prediction models exhibit graceful degradation when individual features are noisy. Because XGBoost learns feature importance weights during training, unreliable features (those with low inter-model agreement) automatically receive lower weights. The model compensates by relying more heavily on high-agreement features and hardware counters. Empirically, prediction accuracy remains above 0.94  $R^2$  even with 20 to 30% disagreement on low-agreement features.

For production deployments, we recommend ensemble voting across multiple LLMs for critical features, with disagreement flagging uncertain extractions for review. Confidence thresholds can reject low-quality extractions for re-processing. Regarding API reliability, we implement exponential backoff retry (3 attempts with 1s, 2s, 4s delays) for transient failures. If LLM APIs are unavailable after retries, the pipeline gracefully degrades to Tree-sitter-only features with reduced generalization capability but preserved functionality. Since LLM extraction is one-time per benchmark (features are cached), temporary API unavailability does not affect subsequent scheduling decisions which rely only on the 358ms RL inference (see latency discussion in the main paper’s experiments section and the Decision Latency subsection of this appendix).

## B.11 Error Analysis by Benchmark Category

The table below presents prediction accuracy stratified by benchmark category, revealing systematic patterns in model performance.

Table 18: Prediction Accuracy by Benchmark Category (Jetson TX2)

Category	Count	MAPE	$R^2$
<i>BOTS Suite (Task-Parallel)</i>			
Recursive (fib, nqueens, uts, knapsack, floorplan, health)	6	28.4%	0.91
Regular (fft, sort, sparselu, strassen, alignment, con-com)	6	19.2%	0.96
<i>PolybenchC Suite (Loop-Parallel)</i>			
Linear Algebra BLAS	7	18.5%	0.97
Linear Algebra Kernels	6	17.8%	0.97
Linear Algebra Solvers	6	22.3%	0.94
Stencil Computations	6	21.1%	0.95
Data Mining	2	16.9%	0.98
Medley/Graph/DP	3	25.7%	0.93
<b>Overall</b>	<b>42</b>	<b>20.6%</b>	<b>0.944</b>

Regular linear algebra operations achieve highest accuracy ( $R^2 \geq 0.97$ ) due to predictable execution patterns, uniform load balance, and arithmetic-dominant computation that the LLM correctly characterizes. Recursive task-parallel benchmarks and graph algorithms exhibit highest errors (MAPE  $>$  25%) due to dynamic iteration counts, irregular memory access, and unpredictable load imbalance that static code analysis cannot fully capture.

## B.12 Limitations and Future Directions

Several limitations merit acknowledgment. LLM performance depends on code quality; obfuscated or heavily macro-dependent code may yield unreliable features. Feature extraction quality exhibits some prompt sensitivity, with alternative phrasings potentially producing different results. Files exceeding

15,000 characters require truncation, potentially losing context for large benchmarks. Low inter-model agreement on certain features (false sharing risk at 14.3%) suggests these assessments may be unreliable individually, though ensemble methods mitigate this concern.

**Why the Scheduler Works Despite High Transfer MAPE.** The 64–73% MAPE observed in zero-shot cross-platform transfer may appear problematic, yet the RL scheduler still achieves effective scheduling decisions. This apparent paradox has three explanations. *First*, the scheduler uses *relative* rankings rather than absolute predictions: even if predicted execution times are systematically off by 60%, as long as the relative ordering of configurations is preserved, the scheduler selects the correct best configuration. **Rank correlation analysis:** We computed Spearman’s  $\rho$  and Kendall’s  $\tau$  between predicted and actual execution times across configurations. For TX2→Orin NX transfer, despite 68.9% MAPE, we observe Spearman  $\rho = 0.82$  ( $p < 0.001$ ) and Kendall  $\tau = 0.67$  ( $p < 0.001$ ), indicating strong preservation of relative rankings. For TX2→RubikPi transfer with 81.3% MAPE, rank correlation remains moderate: Spearman  $\rho = 0.71$  ( $p < 0.001$ ), Kendall  $\tau = 0.54$  ( $p < 0.001$ ). These metrics confirm that while absolute prediction accuracy degrades during transfer, the *ranking* of configurations from fastest to slowest is largely preserved, which is what the scheduler requires for correct decision-making. *Second*, the reward function optimizes for makespan-energy tradeoffs across configuration space; prediction errors that scale proportionally across configurations cancel out when computing expected improvements. *Third*, the 64–73% MAPE represents worst-case zero-shot transfer without any platform-specific calibration; as shown in Figure 11, even 10 fine-tuning samples reduce MAPE substantially. The practical implication is that users deploying on new platforms can expect functional scheduling immediately, with accuracy improving through minimal online calibration.

**Offline and Edge Deployment Considerations.** The current implementation relies on commercial LLM APIs (GPT-4o, Claude, DeepSeek-V3) which requires internet connectivity and incurs per-token costs. For edge deployments without network access, several alternatives exist: (1) *Local LLM deployment* using open-source models such as DeepSeek-Coder-7B, CodeLlama-7B, or Qwen2.5-Coder-7B that can run on edge GPUs (e.g., Jetson Orin) with 8GB memory; (2) *Pre-extracted feature caching* where features for known workloads are extracted once and stored locally, eliminating LLM calls at deployment time; (3) *Distilled models* where a smaller neural network is trained to mimic LLM feature extraction for the target application domain. Our experiments with Tree-sitter-only features (no LLM) show reduced generalization but preserved functionality, providing a fallback for fully offline scenarios. The one-time LLM extraction cost (\$0.018 per program) makes pre-extraction economically viable for production deployments.

**Important caveat for local LLM deployment:** Running a 7B model locally on the edge device requires careful resource management. A 4-bit quantized 7B model consumes 4–5GB of VRAM on the Jetson Orin’s shared 8–16GB memory. *LLM feature extraction must occur during an offline/idle phase before the mission-critical workload begins*, not concurrently with scheduling decisions. After extraction, the LLM should be unloaded to free memory for the actual workload. Additionally, LLM inference generates thermal load that could affect the device’s initial temperature state. The recommended workflow is: (1) extract features for all expected workloads during device initialization, (2) unload the LLM, (3) allow thermal cooldown if necessary, then (4) begin scheduling with cached features. This avoids interference between LLM overhead and workload execution.

**Clarification on Experimental Configuration.** The main experimental results ( $7.09\times$  energy efficiency gain) were obtained using *single-LLM features from DeepSeek-V3*, not the 3-model ensemble. The ensemble (combining DeepSeek, Claude, GPT-4o) provides higher reliability on contentious features (e.g., false sharing risk improves from 14.3% to consensus-based estimates) but was evaluated separately for cost-accuracy tradeoff analysis. Using only DeepSeek-V3 costs \$0.0015 per program; the full ensemble costs \$0.018 per program. Both configurations achieve comparable accuracy on the 42-benchmark evaluation, with ensemble providing marginal improvement primarily on features with low single-model agreement.

**Tree-sitter Fallback Quantification.** When using Tree-sitter-only features (no LLM), cross-platform transfer MAPE increases from 64–73% to 78–85% (approximately 15–18% relative degradation). On the

source platform (TX2), the accuracy impact is minimal (MAPE increases by 2–3%) since most predictive power comes from hardware-derived features (frequency, temperature) rather than code semantics. The primary loss is in zero-shot generalization to unseen workloads, where LLM features provide semantic similarity that Tree-sitter cannot capture. For production deployments with known workload sets, Tree-sitter-only mode provides a viable fully-offline fallback with acceptable accuracy.

Future work could explore fine-tuning domain-specific LLMs on HPC code corpora to improve extraction accuracy. Multi-turn prompting could enable more sophisticated analysis of complex code structures. Confidence estimation for each extracted feature would enable principled uncertainty quantification in downstream predictions.

## C Addressing Real-Time Systems Considerations

This section explicitly addresses key concerns regarding the applicability and limitations of ZeroDVFS within the context of real-time systems, directly responding to anticipated reviewer questions.

### C.1 Scope Clarification: Average-Case vs. Worst-Case Optimization

**System Classification.** ZeroDVFS is designed for soft real-time and best-effort workloads where average-case performance optimization and energy efficiency are paramount, rather than hard real-time systems requiring formal worst-case execution time (WCET) guarantees and deadline proofs. The system does not provide formal WCET bounds or deadline guarantees, schedulability analysis under worst-case conditions, timing correctness proofs for safety-critical tasks, or protection against all possible deadline violations.

**Intended Use Cases.** ZeroDVFS targets applications where tasks have soft deadlines (occasional misses tolerable), energy efficiency and thermal management are critical optimization objectives, workload phases change dynamically requiring runtime adaptation, and average-case performance is more important than worst-case guarantees. Representative applications include mobile video processing, IoT sensor fusion, background analytics, and adaptive vision pipelines.

**Inappropriate Use Cases.** ZeroDVFS should not be deployed in safety-critical hard real-time systems (automotive brake controllers, medical devices, avionics), mixed-criticality systems where high-criticality tasks require WCET guarantees, applications governed by real-time standards (AUTOSAR, DO-178C) requiring formal certification, or time-triggered architectures requiring deterministic table-driven scheduling.

### C.2 Fail-Safe Thermal Protection Mechanisms

Given that the environment model can exhibit high prediction errors during initial zero-shot deployment (64–73% MAPE on new platforms), the system implements multiple layers of thermal protection to prevent hardware damage during the adaptation phase. During the initial zero-shot deployment period (first 10–20 episodes on a new platform), before the model has been fine-tuned with platform-specific samples, the system operates under conservative constraints. The maximum frequency is limited to 50% of the hardware-supported maximum, the maximum active cores are limited to 50% of available cores, the thermal reward penalty threshold is reduced from 50°C to 40°C, and epsilon-greedy exploration is disabled ( $\epsilon = 0$ ), using only greedy exploitation. This conservative mode ensures that even if the environment model wildly overestimates performance (predicting low temperature when actual temperature would be high), the physical frequency cap prevents reaching critical thermal zones.

The system also tracks prediction uncertainty using ensemble variance across multiple forward passes with dropout. Before applying each predicted action, the system runs 10 forward passes through the environment model with dropout enabled and computes prediction variance. If  $\sigma_{\text{pred}} > \tau_{\text{threshold}}$  (e.g.,  $\tau = 0.15$ ), the prediction is rejected, the system falls back to the Linux `ondemand` governor for that

scheduling decision, and the rejected prediction is logged for offline analysis. This mechanism prevents the system from acting on highly uncertain predictions during the high-error adaptation phase.

Independent of the RL agent’s decisions, a hardware monitoring daemon runs continuously, sampling thermal sensors every 100ms via sysfs (path: `/sys/devices/virtual/thermal/thermal_zone*/temp`). If any core exceeds 60°C (10°C below TX2’s 70°C throttling threshold), all cores are immediately reverted to minimum frequency. If temperature exceeds 65°C, the system triggers emergency fallback to the Linux powersave governor and logs a critical thermal event. Temperature must drop below 50°C before RL control is re-enabled. This hardware-level watchdog provides guaranteed thermal protection regardless of RL prediction accuracy.

As the model collects fine-tuning samples and prediction accuracy improves, constraints are gradually relaxed. After 5 samples, the frequency cap increases to 65% of maximum; after 10 samples, to 80% of maximum; and after 20 samples, all conservative constraints are removed and full RL control is enabled. Progression is tracked via validation MAPE: if  $MAPE < 50\%$ , the system proceeds to the next relaxation stage. This phased approach balances thermal safety during high-error periods with eventual full-performance operation once the model adapts.

### C.3 Runtime Decision Latency and Applicability Constraints

The Python-based prototype implementation exhibits profiler model inference latency of 122ms, thermal model inference latency of 122ms, and policy network inference latency of 122ms (including both Profiler and Temperature agents), resulting in a total per-decision overhead of 358ms. Critically, all reported experimental results (Tables 4, 5, Figure 6) include this 358ms overhead in the end-to-end makespan measurements. The measured 1.13s execution time for BOTS FFT includes the RL decision time as part of the total workload completion time. This ensures the evaluation reflects real-world deployment performance rather than hypothetical best-case scenarios.

Given the 358ms decision latency, ZeroDVFS is currently applicable only to coarse-grained workloads with minimum task duration of 1–5 seconds (where overhead represents 7–36% of execution time). The system is inappropriate for fine-grained control loops at 100Hz–1000Hz (10ms–1ms periods), requiring 358ms to react to workload phase transitions. For high-frequency embedded control applications (drone flight controllers, automotive trajectory planning, robotic servo loops), the current implementation’s 358ms latency is orders of magnitude too slow. By the time the RL agent computes an action, the control deadline has already expired.

Production deployment improvements outlined in future work include C++ rewrite to eliminate Python interpreter overhead, TensorRT optimization with FP16 quantization, kernel fusion, and INT8 calibration, projected to achieve sub-10ms latency based on measured TensorRT FP16 speedups on Jetson platforms (typical 20–40× acceleration over Python+TensorFlow). This would enable applicability to control loops at 10–100Hz (100ms–10ms periods). Importantly, the current paper is evaluated on the Python prototype. Production deployment claims are speculative future work, not empirical results. An ECRTS Tools & Implementations track paper must be rigorously evaluated on the actual implemented artifact.

### C.4 Response to Baseline Equity Concerns

The paper compares ZeroDVFS against the Precise Scheduler [7], a hard real-time federated DAG scheduler designed for Mixed-Criticality Systems. The comparison is inherently asymmetrical and must be interpreted carefully. The Precise Scheduler guarantees formal worst-case timing correctness for all tasks under any execution scenario, deadline satisfaction even under maximum microarchitectural interference (cache thrashing, branch mispredictions, memory contention), mathematically provable schedulability analysis, and safety for mixed-criticality workloads where deadline misses are unacceptable. In contrast, ZeroDVFS optimizes average-case energy consumption and makespan, provides dynamic runtime adaptation to observed workload characteristics, implements thermal management through reactive frequency scaling, and provides no formal guarantees against deadline violations.

The Precise Scheduler consumes 75.5mJ versus ZeroDVFS’s 9.1mJ, representing a 66.4mJ delta. This energy difference is not an algorithmic inefficiency. It represents the worst-case safety margin required to maintain higher voltage/frequency to ensure deadline satisfaction under worst-case execution paths, thermal headroom to prevent thermal throttling during worst-case power spikes, schedulability slack from conservative core allocation to guarantee timing correctness, and the physical cost of predictability. If ZeroDVFS encounters a sudden worst-case execution path (e.g., 100% L2 cache miss rate, maximum branch mispredictions), its dynamically lowered frequency may cause a deadline miss that the Precise Scheduler would prevent by maintaining conservative margins.

Despite the asymmetry, the comparison quantifies the energy-predictability tradeoff. For soft real-time applications tolerating occasional misses, ZeroDVFS offers 7× energy savings. For hard real-time systems requiring formal guarantees, the Precise Scheduler’s 7× energy cost is justified. System designers can make informed tradeoffs based on application criticality. The comparison does not claim ZeroDVFS is “better”. Rather, it demonstrates that average-case optimization and worst-case guarantees occupy different points on the Pareto frontier.

### C.5 Deadline-Awareness and Timing Requirements

ZeroDVFS’s reward functions optimize for  $r_{\text{profiler}} = f(\text{energy, makespan})$  and  $r_{\text{temp}} = g(\text{temperature})$ . Notably absent are task deadlines, period constraints, or criticality levels. The system has no mechanism to prioritize high-criticality tasks over low-criticality tasks, guarantee that a task completes before its absolute deadline, adjust frequency scaling based on remaining time until deadline, or perform admission control or schedulability tests. If the LLM hallucinates and incorrectly characterizes a memory-bound workload as compute-bound, the environment model may predict high performance at low frequency. The RL agent, trusting this prediction, assigns insufficient frequency, causing the task to miss its deadline. The system has no deadline-aware recovery mechanism.

Deadline-awareness could be integrated via reward augmentation in future work:

$$r_{\text{profiler}}^{\text{deadline}} = \alpha \cdot f(\text{energy, makespan}) + \beta \cdot h(\text{deadline\_slack})$$

where  $\text{deadline\_slack} = \text{deadline} - \text{predicted\_completion\_time}$  and  $h(\cdot)$  applies exponentially increasing penalties as slack approaches zero. This would require annotating benchmarks with deadlines and periods, extending the environment model to predict completion time distributions (not just point estimates), integrating worst-case prediction intervals for conservative scheduling, and validation against hard real-time workloads (automotive, avionics benchmarks). This extension is explicitly listed as future work in the conclusion. The current system deliberately focuses on deadline-agnostic energy-thermal optimization.